Search for cold dark matter by means of large inorganic scintillators

Ken-ichi Fushimi

DISSERTATION IN PHYSICS

THE OSAKA UNIVERSITY
GRADUATE SCHOOL OF SCIENCE
TOYONAKA,OSAKA

Contents

Abstract

Large inorganic scintillators have been developed to search for WIMPs by measuring elastic and inelastic scattering from Na and I nuclei in the scintillators. WIMPs (Weakly Interacting Massive Particles) are thought to be the most probable dark matter candidates. They have been proposed in views of astrophysics and particle physics.

First, the light output response of nuclear recoil is indispensable value in order to search for WIMPs by direct method. It was obtained by measuring the inelastic excitation and elastic scattering by fast neutron from ^{252}Cf. The relative response is defined as $f = E_o/E_R$, where E_o is the observed electron equivalent energy and E_R is the kinetic energy of the recoil nucleus. The f values for I and Na nuclei were determined as $f_{\rm I} = 0.05 \pm 0.02$ and $f_{\rm Na} = 0.4 \pm 0.2$, respectively.

Huge NaI(Tl) scintillators of the high sensitivity low background detector system ELEGANTS V were applied to search for WIMPs. A low noise ($\sim$ 5keV) and a low background ($\sim$ 8/day/keV/kg) were achieved even with a large (36.5kg) NaI(Tl) scintillator. NaI is shown to have merits of a large volume, large scattering cross sections for WIMPs and of 100% abundance of the finite-spin nucleus. It, however, has a demerit of a small form factor due to the finite-size effect of ^{127}I at the present observed energy region. This experiment made sure that the scintillation detector can be used for the direct detection of DM.

The axial-vector excitation of ^{127}I by inelastic scattering of WIMPs was studied to search for spin-coupled WIMPs. The inelastic process from ^{127}I has advantages of a large cross section, a large scintillation output (noise free) and a known nuclear matrix element. In the present work $E^* \simeq 60$keV was analyzed for the same data which were used to study the exotic K X-rays. The NaI detector consists of 20 modules of 10.2cm$\times$10.2cm$\times$101.6cm NaI(Tl) crystals. Energy spectra, for the live time of 1818 hours, from the 17 of the NaI modules were summed for the final energy spectrum. Stringent limits by direct measurements were obtained on the purely spin-coupled WIMPs candidates.

A CaF_2(Eu) was shown to be a quite suitable detector to search for spin-coupled WIMPs. The ^{19}F nucleus has the advantage of a large and calculable matrix element of elastic scattering. The properties of a CaF_2(Eu) and a CaF_2(pure) have been studied. The large detector system of the CaF_2(Eu) has been developed. The goal of this system is to set strong limit as $\Omega_\chi < 10$ by elastic scattering and $\Omega_\chi < 1$ by the annual modulation. It was shown that the effective limit on the density of ν_D and ν_M will be given by a few years long measurement of the annual modulation.

Chapter 1

Introduction

1.1 Rare decay physics and the dark matter

Recently, many interesting experimental studies have been carried out in the field of non-accelerator physics. They were developed to investigate the rare decay physics such as $\beta\beta$ decays, dark matter, and the possible violations of fundamental laws. They have provided one with valuable information on particle, nuclear and astrophysics, which cannot be obtained by the accelerator physics.

1.1.1 Dark Matter Problem

The dark matter problem is one of the most important subjects in astrophysics and particle physics view points. There are several indications that the universe contains a large amount of the DM [1]. When a density ρ of the matter in the universe is discussed, it is convenient to compare all the densities to the critical density,

$$\rho_c = \frac{3H_0^2}{8\pi G} \simeq 1.05 \times 10^4 h^2 \text{ eVcm}^{-3}, \tag{1.1}$$

where $H_0^{-1} = 9.8 \times 10^9 h^{-1}$yr and $0.5 \leq h \leq 1$. The universe will expand forever in case of $\rho \leq \rho_c$, whereas the expansion will turn to the collapse in case of $\rho \geq \rho_c$. It is conventional to define

$$\Omega \equiv \rho/\rho_c. \tag{1.2}$$

The first dark matter problem comes from many estimations of the dynamical/luminous mass ratio of the galaxies. The mass of the luminous matter (radiate detectable light) of the galaxies has been estimated by measuring the number of galaxies and stars in the galaxy. These estimates give the lower bound of the density, $\Omega \simeq 0.01$. On the other hand, the dynamical mass has been measured by the velocity distribution of the galaxy rotation and relative motion of the galaxies in the galactic clusters.

First, the dynamical density of matter ($\Omega_{\rm DYN}$) in the galaxy has been estimated by the observations of the galaxy rotation Masses and mass distributions have been determined from the rotation velocity curves of the galaxies. The masses depend on the models: i) disk galaxy models, which give lower limits to the masses, ii) spherical galaxy models, which give upper limits to the masses. The non-luminous matter is shown to extend beyond the luminous region. The mass of the non-luminous halo amounts to almost 90% of the total mass of the galaxy. Many facts for such a massive dark halo of the galaxies are reported [1][3][4].

Second, an estimate for the existence of a dark massive cluster was reported [5]. They observed the relative motion of the galaxies in the galactic cluster, named Eridanus A. This cluster contains only two bright galaxies. It has a large mass which is determined by their velocity dispersion. It has a large mass-to-light ratio $M/L \simeq 3000h$, which makes it one of the darkest clusters known so far. Such dark clusters with $M/L \simeq 3000h$ can exist and even be numerous.

From these facts, the existence of dark matter is quite reliable. The mass ratio Ω which is obtained from the studies of the dynamics of galaxy halos, groups and clusters of galaxies has been inferred that $\Omega_{\rm DYN} \simeq 0.1 \sim 0.3$.

The another dark matter problem comes from the baryon density limit. The nucleon density in the universe may be related to the nucleon-photon ratio $\eta_{10} \equiv$

$N/10^{10}\gamma$ and the temperature of the cosmic microwave background (CMB) as,

$$\Omega_{\rm B}h^2 = 3.7 \times 10^{-3}\eta_{10}(T/2.74{\rm K})^3. \tag{1.3}$$

Studies of the abundances of the light elements produced in Big Bang Nucleosynthesis constrain that $\eta_{10} = 3 - 10$ [6] (see table 1.1). Thus one gets $0.01 \leq \Omega_{\rm B} \leq 0.14$. This suggests that $\Omega_{\rm B} \leq \Omega_{\rm DYN}$, which gives the another dark matter problem.

Table 1.1: Constraints of the η_{10} derived by the abundance constraints of the light elements.

Abundance Constraint	Bound on η_{10}
D/H$\geq 1 \times 10^{-5}$	$\eta_{10} \leq 10$
D/H$\geq 2 \times 10^{-5}$	$\eta_{10} \leq 7$
^{7}Li/D$\leq 1.5 \times 10^{-5}$	$\eta_{10} \leq 7$
^{7}Li/H$\simeq 1 \times 10^{-10}$	$2 \leq \eta_{10} \leq 5$
(D+^{3}He)/H$\leq 6 \times 10^{-5}$	$\eta_{10} \geq 4$
(D+^{3}He)/H$\leq 10 \times 10^{-5}$	$\eta_{10} \geq 3$

Theoretical prejudice favors $\Omega = 1$ for these reasons.

1. **The inflation theory**

   This hypothesis is proposed in order to solve many problems in the big bang cosmology. It leads to the prediction of vanishing curvature of the universe, $k = \Omega - \Omega_{\rm vac} - 1 = 0$. Where $\Omega_{\rm vac}$ is the vacuum energy, $\Omega_{\rm vac} = \Lambda/3H^2$. The observational upper limit implies that $\Omega_{\rm vac} = 0$.

2. **Expansion rate**

   In case of Ω is much larger than unity, the expansion rate of the universe is too small to expalin the present expansion rate. This gives the upper bound as $\Omega < 2$. In case of Ω is much smaller than unity, the expansion rate of the universe should be much larger than the observation.

From these arguments, the dark matter is sure to exist and is likely to be non-baryonic matter.

When one discusses the density of the dark matter in the vicinity of the sun, it is estimated from the observation of the rotational velocity of the stars and gas in the galaxy. It should be noted that the halo density component is dominated by the viible matter at smaller galactic radii. In fact, the density of dark matter, which is expected a smooth extrapolation of the density distribution into the galactic center, is a factor 100 smaller than the density of the luminous matter. The mean density of the dark matter at the position of the sun is $0.6\sim0.3\mathrm{GeVcm}^3$. From now on, the density of the dark matter in the vicinity of the sun is taken as $0.3\mathrm{GeVcm}^{-3}$.

1.1.2 Candidates of dark matter

The DM particles are assumed to have only weak and/or gravitational interactions. If they have strong or electromagnetic interactions, they have interacted with the matter in the universe. Thus they cannot spread into the wide area out of the galactic halo. They were proposed in order to resolve the difficulty in the adiabatic perturbation of baryons, i.e. galaxy and their structure formation. The candidates of DM are classified into two large divisions by their mass and their typical velocity, that is to say, relativistic hot dark matter (HDM) and non-relativistic cold dark matter (CDM).

The former is expected to be light particles with the mass of $m_\chi \leq 10\mathrm{eV}$. They decoupled with photons at the relativistic stage. In HDM scenario, a characteristic scale length is as large as the scale of superclusters of galaxies. The fluctuation which creates small structure is erased. This nature causes the difficulty that all the galaxies are concentrated in superclusters, which does not agree with the observation.

The candidates of the HDM particles such as light massive neutrinos (GUT)

and others have been proposed by particle physics. The most probable HDM candidate is light neutrinos. In the framework of the standard electro-weak theory, the neutrino is a massless particle. But it can have a finite Majorana mass and/or the right handed weak current term in theories beyond the standard theory (ex. GUT). Measurement of the neutrino-less double beta decay is the quite sensitive check of the Majorana mass of the neutrino. The limits on the half life of the neutrino-less double beta decay have been studied extensively by double beta decays [10][11][39]. The upper limits on the mass of electron neutrino are $< m_\nu >< 7$eV from ^{100}Mo [39], $< m_\nu >< 5.5$eV from ^{116}Cd [11] and $< m_\nu >< 1.1$eV from ^{76}Ge [10].

The other candidates of the dark matter are expected to be non-relativistic particles. The CDM can explain the creation and growth of the small scale fluctuation of matter density as a seed of the structure of galaxies. If only the CDM exists in the universe as dark matter, the CDM distribution becomes so smooth that the large scale structure cannot be created.

Recently, the mixed dark matter (HDM+CDM) model has been extensively discussed. The observation of the cosmic microwave background (CMB) by COBE (COsmic Background Explorer) satellite [12] has shown statistically significant ($> 7\sigma$) structure that is well described as scale-invariant fluctuations with a Gaussian distribution. They reported that the temperature fluctuation amplitude was $16\pm4\mu$K ($\Delta T/T \simeq 6\times10^{-6}$). This CMB anisotropy has been interpreted with several DM models introducing the mixture of the CDM ($\Omega_{\rm CDM}$), the HDM ($\Omega_{\rm HDM}$) and the baryon density ($\Omega_{\rm B}$) [13] [14]. A model whose parameters are $\Omega_{\rm CDM} = 0.6, \Omega_{\rm HDM} = 0.3, \Omega_{\rm B} = 0.1$ and $h = 0.5$ is shown to give an excellent fit to the observed bulk flow and the CMB anisotropy in both large and small scales [13]. From this point of view, the CDM can be considered as the main component of the dark matter.

The candidates of the CDM particles are the axion, the heavy neutrinos and the

lightest supersymmetric particles (LSPs). The astrophysical limits on the axion mass are examined by the stellar [7] and supernova (SN1987A) cooling rate [8] by a number of authors. The limits on the axion mass, m_a, are $m_a < 0.03$eV from white dwarf cooling rates, $m_a < 0.01$eV from He ignition in red giants and $m_a < 2.8$eV from the SN1987A cooling rate. From the cosmological constraint of $\Omega_a < 1$ the lower limit on the axion mass is calculated from the equation [1],

$$\frac{m_a}{10^{-5}\text{eV}} \simeq 0.83 \times 10^{0\pm0.34} F^{-1}. \tag{1.4}$$

The factor F is given by,

$$F = (h^2\Omega_a)^{0.85}. \tag{1.5}$$

For $\Omega_a = 0.9$ and $h = 0.5$, for example, eq.1.4 gives $m_a > 3 \times 10^{-5}$eV. Thus there is a narrow allowed window between the mass range $10^{-5} < m_a < 10^{-2}$eV. Many experiments to search for the light axions by direct detection have been proposed [9].

The other CDM particles are generally called WIMPs (Weakly Interacting Massive Particles). The motivations of these particles are listed as follows.

1. **Solar neutrino problem**

   Some massive particles are proposed to solve the solar neutrino problem. This problem is the deficit of the solar neutrino from the reaction in the center of the sun. The observation of high energy neutrinos from the sun [15] [16] [17] gives only 50% of the neutrino flux relative to the prediction by the standard solar model. Since the neutrino flux depends on the temperature of the center of the sun, the particle which cools down the central region of the sun was proposed in order to solve this problem. The mass is limited between 4GeV and 10GeV. If its mass is lighter than 4GeV, they 'evaporate' from the sun. And if it is heavier than 10GeV they cannot transport the energy from the center. Cosmion is a typical candidate of these particles [18]. Its

scattering cross section is also limited to give the optimum interaction with the nucleus in the sun.

2. **Particle physics**

   Massive Dirac and Majorana neutrinos are considered as the candidates of the DM. They can have a large mass above 14GeV (10GeV) for $\nu_D(\nu_M)$ if the present Hubble expansion rate is $50\text{kms}^{-1}\text{MPc}^{-1}$. The other candidates of DM come from the supersymmetry theory. The lightest superpartner (LSP) is thought to be stable. The candidates of the LSPs are sneutrinos, photino and other neutralinos. Since these candidates are expected not only from the cosmology but also from the particle physics, studies of these particles as DM candidates are very important from view points of both cosmology and particle physics.

1.2 Cross sections of WIMPs

The WIMPs particle interacts via weak interaction by exchanging Z^0, $W^{\pm}$ or scalar quark ($\tilde{q}$). The WIMPs-nucleus scattering is classified into two types, coherent scattering and spin-dependent scattering. The elastic scattering amplitude for the vector coupling interaction is a coherent sum of the scattering amplitudes over all nucleons (see Fig.1.1 a). On the other hand the elastic scattering amplitude by the axial-vector (spin-coupled) interaction is due to only one single (valence) nucleon with a finite spin J in the odd A nucleus (Fig.1.1 b). Therefore the elastic cross section for the vector-coupled WIMPs is much larger, by approximately a factor of the square of the number of neutrons N_n, than that for the spin-coupled WIMPs [44] [45].

Cross sections for the vector coupled and the axial-vector coupled elastic scat-

tering are written as follows.

$$\sigma_{Coherent} \propto N_k \cdot g_V^2 |F(q)|^2 \tag{1.6}$$

$$\sigma_{Axial} \propto N_k \cdot g_A^2 |F(q)|^2. \tag{1.7}$$

Where N_k is the constant for the k-type DM. The values for N_k are given in table 1.2. The coupling constant g_V and g_A are expressed as

Table 1.2: The constants N_k and the coupling term for the k-type DM particle.

WIMPs	N_k	Coupling term $g_A \cdot G_F$
Dirac Neutrino	$2/\pi$	$\lambda_N(\sum_q T_q^3 \Delta q) \cdot G_F$
Majorana Neutrino	$8/\pi$	$\lambda_N(\sum_q T_q^3 \Delta q) \cdot G_F$
Higgsino	$8\cos^2(2\beta)/\pi$	$\lambda_N(\sum_q T_q^3 \Delta q) \cdot G_F$
Photino	$4/\pi$	$\lambda_N(\sum_q (eQ_q/m_{\tilde{q}})^2 \Delta q)$

T_q^3:the quark isospin, Δq: the spin carried by quark q
Q_q: the charge of quark, $m_{\tilde{q}}$: the mass of squark $\tilde{q}$
$\tan\beta = v_1/v_2$: the ratio of two higgs vacuum expectation values

$$g_V^2 = \left\{N_n - (1 - 4\sin^2\theta_W)N_p\right\}^2 \tag{1.8}$$

$$g_A^2 = 2\lambda_N^2 |\sum_q T_q^3 \Delta q|^2. \tag{1.9}$$

Where N_n and N_p are the numbers of neutrons and protons in the target nucleus, the spin matrix element, λ_N, is expressed with angular momentum eigenstates of the target nucleus as [1],

$$\lambda_N = \frac{J(J+1) + S(S+1) - L(L+1)}{\sqrt{3J(J+1)}}. \tag{1.10}$$

These equations give following informations,

1. In case of the vector coupling WIMPs such as the Dirac neutrino, the scalar neutrino and so on, since $g_V \gg g_V$ for most target nuclei and $4\sin^2\theta_W \simeq 1$,

the cross section is approximately proportional to the square of the number of the neutrons (N_n) in the target (detector) nucleus.

2. In case of the axial-vector coupling WIMPs such as the Majorana neutrino, and so on, since the cross section has only axial vector term g_A, the cross section depends only on the valence nucleon carrying the spin of the nucleus. The values of g_A (λ and Δq) have strong model dependence, but Δq is evaluated by the most recent analysis of the EMC result and the most recent analyses of hyperon decay [47].

There is an inelastic excitation in case of the axial-vector coupling. The low-lying state of target nucleus with excitation energy E^* is excited by the inelastic scattering of WIMPs. It deexcites by a γ-transition, giving the energy deposit E^* (see Fig.1.1 c). This γ-transition energy E^* is transferred to an electron in the detector, and thus is ultimately converted fully to the output response, namely $E_o = E^*$. It should be noted that the excitation energy E^* must be below the kinetic energy E_k of WIMPs, which is of the order of a few hundred keV for $M_\chi \simeq 10^3 - 10^4$GeV and $v_i \simeq 1 - 2 \times 10^{-3}c$.

The cross section for the axial-vector coupled inelastic scattering is written as,

$$\sigma_{Inel} \propto N_k \cdot g_A^2 |F(q)|^2 \frac{p_f}{p_i} f(p_i). \tag{1.11}$$

The spin matrix element for inelastic scattering is expressed as,

$$\lambda_{Inel}^2 = | < A^* | \mathbf{s} | A > |^2, \tag{1.12}$$

where $|A>$ and $|A^*>$ are the ground and excited states and $\mathbf{s}$ is the spin operator.

The spin matrix element in nuclei is hard to calculate accurately because it is sensitive to the spin-isospin correlation. The spin matrix element for elastic scattering has recently been evaluated in terms of the odd-group model[47]. In the

case of the spin-stretched transition to the excited state with spin $J' = J \pm 1$, the spin matrix element is related to the M1γ matrix element of $< A \mid M1 \mid A^* >$ as

$$< A^*|\mathrm{s}|A >= \sqrt{\frac{2J'+1}{2J+1}} \frac{1}{g_M} < A^*|M1|A > . \tag{1.13}$$

Where g_M is the M1 γ coupling constant given by $g_M = \frac{e\hbar}{2M}(\frac{3}{4\pi})^2 \frac{g_s - g_l}{2}$, and the M1 matrix element $< A^*|M1|A >$ is obtained from the transition rate.

1.3 Present status of WIMPs search

1.3.1 Indirect and accelerator search

The limits on the density of the WIMPs candidates have been set by studying high energy neutrinos from the sun due to annihilating WIMPs [19]. The heavy particles whose masses are heavier than a few GeV are captured in the center of the sun and the earth by gravity. They annihilate in the center of them and produce high energy neutrinos. A large neutrino detector is needed to study the flux of neutrinos from the annihilation of WIMPs because the cross section of the neutrino is so small. The large water Čerenkov detector was applied to search for the high energy neutrinos. KAMIOKANDE group has carried out the experiment by a large water Čerenkov detector (3000t of water) to study neutrinos from the sun, the earth and the other objects in the universe. They estimated the expected energy spectra of the high energy neutrinos created by annihilation of WIMPs in the sun and the earth. They excluded the WIMPs candidates in the mass region between 3~150GeV(24~150GeV) for $\nu_D(\nu_M)$ as the main candidates of DM [19]. They have also studied the annihilation of the LSPs in the sun and the earth and have given a stringent limit on the parameter space of μ-ν plane [20].

The accelerator experiments were also analyzed to study the WIMPs candidates [21] [22]. The LEP constraint on Z^0 decays into invisible neutrals is

$$N_\nu \equiv \frac{\Gamma(Z^0 \rightarrow \text{invisible neutrals})}{\Gamma(Z \rightarrow \bar{\nu}\nu)} = 3.09 \pm 0.11$$

if the standard model is assumed for all visible Z^0 decays. If no standard model assumption is made other than the ratio between $\Gamma_{\bar{\nu}\nu}$ and $\Gamma_{e^+e^-}$, the constraint is

$$N_\nu = 2.98 \pm 0.12.$$

These constrains can be interpreted as implying that $N_\nu < 3.22$. The limits on the strength of the coupling of Z^0-WIMPs relative to the coupling of the Z^0-$\bar{\nu}\nu$,

$\sin^2\phi_Z$, are derived by the following relation,

$$0.22 > N_\nu - 3 = \begin{cases} \sin^2\phi_Z \times \beta^{-3} & \text{(Majorana fermions)}, \\ \sin^2\phi_Z \times 4/\beta(3+\beta^2) & \text{(Dirac fermions)}, \end{cases} \quad (1.14)$$

where $\beta = v/c$. The following limits on the WIMPs candidates were derived by Z^0 width [21].

1. ν_D and ν_M with mass less than 42GeV can be ruled out.

2. Neutralinos are probably heavier than 10GeV and they would be a mix of neutralinos.

3. Exotic particles such as cosmions are ruled out.

1.3.2 Direct search

The direct method of searching for WIMPs is very important because it is the *direct* test of the existence of WIMPs. Moreover, this method is possible to select the most favorable target nucleus. The direct search of WIMPs has been applied to low background detectors. In this method, one measures the recoil energy given by WIMPs-nucleus elastic scattering. The methods of measuring the recoil energy are listed below.

1. Ionization detector

2. Bolometer and phonon detector

3. Scintillation detector

The present status of these methods are described below.

Ionization detector.

The ultra low background Ge detector for $\beta\beta$ decay experiment was applied to search for WIMPs [23] [24]. The Ge detector has the great advantage of good energy resolution and small noise. Thus it is quite easy to distinguish backgrounds of low energy X rays. They have excluded the ν_D with the mass between 10GeV and 4.7TeV from the main component of the DM ($\rho_\chi < 0.3\mathrm{GeVcm}^{-3}$) [23][24][26].

For spin-coupled WIMPs, the small abundance of the odd-A nuclei (^{73}Ge; 7.8%) is the greatest disadvantage. Now UCSB/ CfPA/ LBL/ STANFORD/ BAKSAN group is planning to search for spin-coupled WIMPs with three Ge detectors; natural Ge, enriched ^{73}Ge and enriched ^{76}Ge [26]. Since spin-coupled WIMPs hit only ^{73}Ge, the energy spectra may differ each other.

Bolometer and phonon detection.

Recently a bolometer and a phonon detector have been applied to search for WIMPs. They measure the temperature rise caused by nuclear recoil. The specific heat of a crystal which is cooled to a few mK depends on T^3, where T is the temperature of the crystal. Thus the temperature rise so large that it is detectable. They report that the energy resolution are relatively good (ex. FWHM=1.7keV for ionization and 1.9keV for phonon at 60keV [26] [27]).

The best property of this method is the high selectability of recoil and electron events. They can distinguish the recoil and electron events when the ionization and phonon energy signals are analyzed simultaneously. They reported that the electron and recoil events can be clearly divided each other. Thus they can select only the recoil events. However this type of discrimination has been carried out only by Ge crystal. It is not feasible for the other crystal which cannot observe the ionization (ex. LiF crystal [27]). Moreover, they have some disadvantages that this system has to be cooled as 0.03K and there are some difficulties of cooling and operate with a large crystal.

Scintillation detector.

Recently, applications of a large volume scintillator have been made by some groups [28] [29]. A scintillation detector has many advantages of search for WIMPs. Particularly NaI(Tl) and CaF_2(Eu) have large cross section of spin-coupled WIMPs-nucleus elastic scattering. A NaI(Tl) scintillator has a good property that it can distinguish the recoil and the electron events by analyzing the decay time of the photon signal [28]. A scintillation detector is easily applied with large detector system. In fact, our group has applied huge NaI(Tl) scintillator with each mass of 36.5kg and the total mass of 730kg.

In this article, it will be shown that the CaF_2(Eu) scintillation is the quite good detector for spin-coupled dark matter. It has the great advantages of large cross section of WIMPs, large light output and easiness of handling. We are now constructing the large volume CaF_2(Eu) (7.27kg). The properties of the detector system will be shown after.

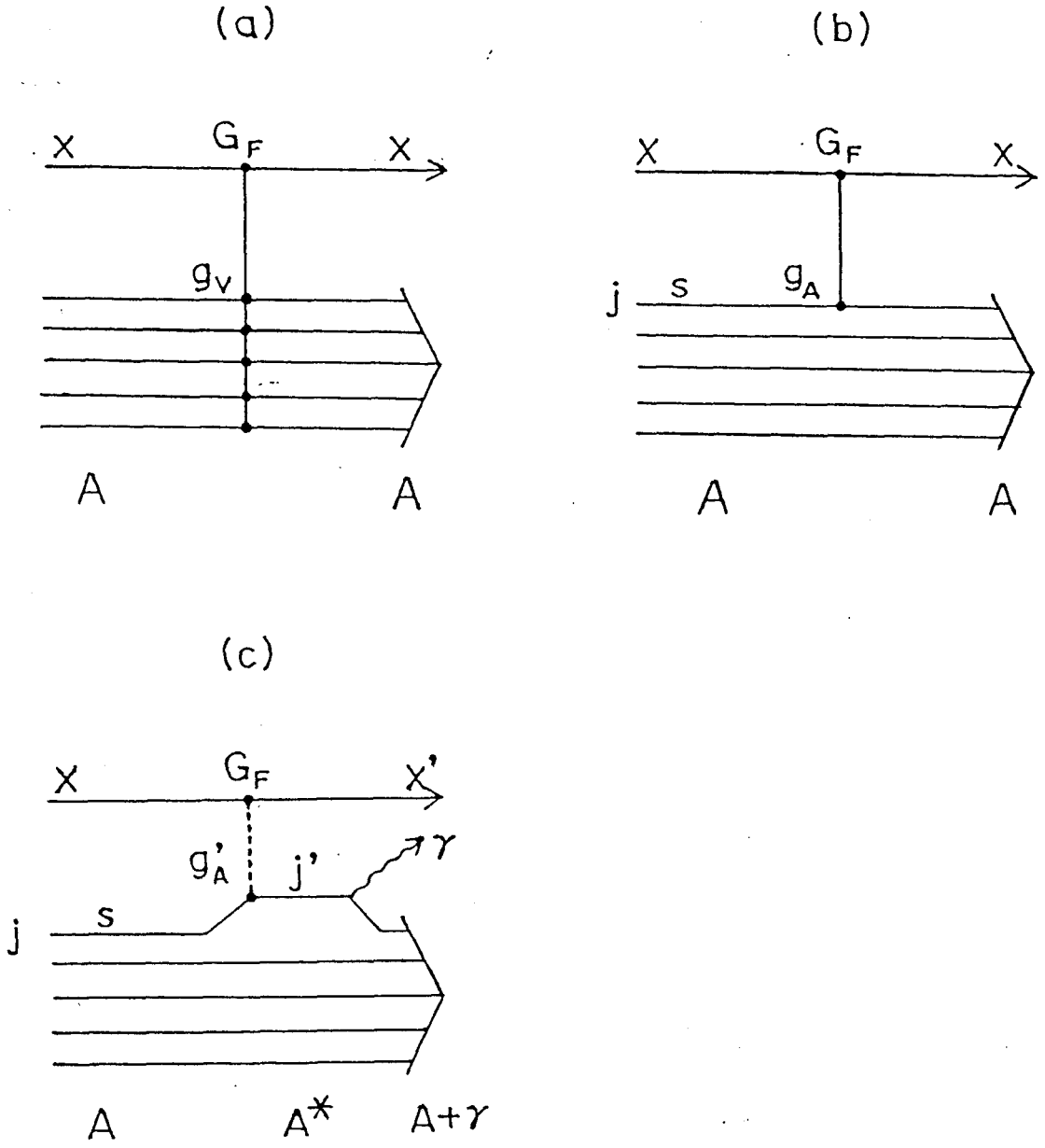

Figure 1.1: Scattering of DM (x) from a nucleus A.
(a) Elastic scattering of vector-coupled DM.
(b) Elastic scattering of axial-vector (spin-coupled) DM interacting with one valence nucleon in j orbit.
(c) Inelastic scattering of axial-vector (spin-coupled) DM, exciting one valence nucleon from j to j' orbits.

Chapter 2

Light output response of nuclear recoil

2.1 Introduction

When a DM particle hits a nucleus in a detector, the recoiling nucleus makes subseqent collisions with atoms. These subsequent collisions can ionize and/or excite electrons of the atoms. In case of a scintillation detector, the following deexcitation processes create scintillation light. However the ionization and excitation by nuclear recoil is quite inefficient than that by electron. Thus only the small fraction, f, of the recoil energy is observed. The observed electron equivalent energy (pulse height) E_o is, for simplicity, given as

$$E_o = f \times E_R, \tag{2.1}$$

where E_R is the recoil energy and f is the conversion (reduction) factor of the pulse height for the recoiling nucleus with respect to the electron.

For ionization detector, Sadoulet et al [31] have reviewed the ionization efficiency. The experimental results of neutron scattering of Ge and Si were analyzed to obtain fs for recoiling Ge and Si nuclei. The fs are consistent with Lindhard's theory [30]. Recently, Ge crystal has been applied to a phonon detector [32]. They measure the phonon signal and ionization signal simultaneously with a 60g of Ge crystal. Since the recoil energy is shared mostly by phonon and less by ioniza-

tion, the pulse of electrons and neutron recoil can be clearly separated. The ratio $E_{phonon}/E_{ionization}$ which gives the ionization efficiency f leads to $f = 0.25$ and this value is consistent with previous estimation by Sadoulet [31]. In case of a scintillator, since the process of the light emission is complex, Lindhard's theory may not be applied. Thus the measurement of the light output response of nuclear recoil of NaI(Tl) is quite important.

2.2 Experiments

The light output responses f for Na and I were obtained by measuring the pulse-height spectrum of recoil nuclei. The measurement was performed by inelastic scattering and elastic scattering of fast neutrons from the ^{252}Cf source with a small (2.5cm $\phi \times$0.5cm) NaI(Tl) detector. The NaI(Tl) crystal was connected with a PMT (H1161;Hamamatsu Co. Ltd.) by optical grease. The recoil energy by the neutron ($E_n \simeq$ a few MeV) scattering gives the same recoil energy by the DM scattering ($E_R \leq$ 100keV).

The fast neutron from ^{252}Cf (2×10^4neutrons/sec) was used. In order to absorb the γ rays from the neutron source, a 1.5cm thick OFHC (Oxygen Free High-conductive Copper) plate and 2cm thick lead plate were placed in front of the detector. The thickness of the absorber was determined by the event rate of NaI(Tl). High energy γ rays from the neutron source can easily be absorbed by lead plate. A copper plate had to be placed between lead plate and the detector to absorb X rays from lead, because the X rays partly overlapped the γ ray of the excited state of ^{127}I. After the γ ray was reduced enough, the event rate was mainly due to the neutron scattering. Multiple scattering effects of neutron are negligibly small in the detector because of its small size.

Two types of the experiments were done to observe inelastic scattering and elastic scattering. In the former experiment, the γ ray from the first excited state

of ^{127}I ($7/2^+$,57.6keV) was observed. The total light output is the sum of the light created by γ ray and that by nuclear recoil, $E_o = E^* + fE_R$, where E_o and E^* are the observed light output and the light output due to the γ ray of the excited state, respectively. Therefore, following two evidences are expected to be observed: (i) the position of the peak shifts to higher energy; (ii) the shape of the peak deforms due to the recoil energy.

In the latter experiment, the elastic scattering of ^{23}Na and ^{127}I were observed. The low energy spectrum is expected to be composed by the elastic scattering spectra of recoil Na nuclei and recoil I nuclei. Since the mass of the ^{127}I nucleus is four times heavier than that of the ^{23}Na nucleus, the shapes of the recoil spectra are much different. The ^{127}I recoil spectrum may fall quickly and the ^{23}Na recoil spectrum may spread over broad energy region ($\leq$ 100keV). Each result was compared with the Monte Carlo simulations which were demonstrated with various values of f. The χ^2 were calculated and the most probable value of f was given when the χ^2 was minimized.

Since quite precise measurement was needed, the following attentions were required during the measurement.

1. **Temperature control.**

   The energy-ADC channel relationship varied slightly with the temperature. This effect likely spoils the analysis of the peak-shift. The effect of the change in the room temperature was carefully examined. Finally, it was shown that the effect was negligible when the room temperature was kept the fixed room temperature by an air-conditioner.

2. **Event rate and peak shift.**

   The energy-pulse height relationship may vary when the event rate extremely differs between each measurement. Actually, the peak position varied when

the event rate was 100cps and when it was 2000cps. The event rate was unified to 960cps, which was limited by the weakest γ source.

2.2.1 Result I (Inelastic scattering)

During the irradiation of the neutron, the γ ray peak from the first excited state, 57.6keV ($7/2^+ \rightarrow 5/2^+$; M1 transition), was remarkably seen. The half-life of this state is so short (1.9ns) that the light due to γ ray and the light due to nuclear recoil are added each other. Thus the precise measurement of the shift of the peak and the tail of the peak was carried out.

First, the shift of the peak position was studied. Since the accurate measurement of the small shift of the peak was needed, linearity in the light output was examined by using ^{137}Cs (31keV K-X ray), ^{133}Ba (32keV K-X ray and 81keV γ ray), ^{210}Pb (46.5keV γ ray), and ^{241}Am (59.5keV γ ray) sources. The ADC channel-energy relationship is shown in Fig.2.1. The peak positions are calculated by gaussian fitting. The calibration shows quite good linearity (correlation coefficient $r = 0.9999$). The peak position of the inelastic excited γ ray peak was also plotted. Since this peak has a small tail due to the recoil of ^{127}I nucleus, the peak position was the top of the peak. The peak shift agrees the Monte Carlo simulation which was performed with the parameter $f = 0.05$.

Next, the shape of the peak was analyzed. The peak of 57.6keV γ ray is expected to have a small tail at higher energy side. However, this tail is quite small if the light output response is small. Thus the measurement was performed for the live time as long as 90000sec in order to get good statistic accuracy . It corresponds the statistical accuracy of 0.7%.

The energy resolution in the measured energy region must be small enough to observe the slight deformation of the peak. The energy resolution was determined by interpolation from the measured energy resolutions by several γ rays (32keV,

46.5keV, 59.5keV and 81keV). The energy resolutions at the several energies are listed in table2.1.

Table 2.1: The measured energy resolutions (FWHM) of the NaI(Tl).

Source	Energy (keV)	ΔE(keV)
^{133}Ba	31	7.53
^{137}Cs	32	7.62
^{210}Pb	46.5	8.94
^{241}Am	59.5	9.41
^{133}Ba	81.0	11.13

The observed peak at the energy of 57.6keV (^{127}I), which is shown in Fig.2.2, is due to the inelastic scattering of $^{127}\mathrm{I}(n,n')^{127}\mathrm{I}^*$. The peak shows a tail at higher energy side due to the additional recoil energy of ^{127}I. The peak was simulated by the sum energy spectrum of E_o(=57.6keV+$f_I \cdot E_R$) with the measured energy resolution of 9.2keV(FWHM) using Monte Carlo method, where the recoil energy (E_R) of $^{127}\mathrm{I}^*$ is calculated by the kinematics of ^{127}I(n,n')^{127}I*(57.6keV) reaction. The energy spectrum of neutrons from ^{252}Cf was assumed to obey Maxwellian distribution with the mean energy of 2.35MeV. The angular distribution of the differential cross section was taken into account, the distribution is isotropic in the center-of-mass system[34]. The systematic error was calculated by the χ-square with various values of f_{I}. The peak was well reproduced with the factor $f_{\mathrm{I}} = 0.05 \pm 0.02$ as shown in Fig.2.2.

2.2.2 Result II (Elastic scattering)

In order to measure the light output response for ^{23}Na recoil and to confirm the result of ^{127}I by inelastic scattering, the elastic scattering of Na nuclei and I nuclei were also studied.

Three types of data were taken;(i) the background before irradiation (**RUN-A**), (ii) the foreground (**RUN-B**), (iii) the background after irradiation (**RUN-C**).

From the RUN-A data, a noise of a PMT was found below a few tens keV. Since this continuous noise has a large influence on the analysis, it was subtracted from all the spectra.

The background, RUN-C, was analyzed to find the activated backgrounds which were produced by fast neutrons from the neutron source. The energy spectra were stored every 5 minutes and the change of the spectrum was studied. There was a prominent peak at 28keV. It is the X ray from ^{128}I produced by neutron capture of ^{127}I. Its intensity decreased the lapse of time whose half life was $T_{1/2} = 26.5 \pm 3.8(1\sigma)$min (see Fig.2.3). It agrees with the half life of ^{128}I ($T_{1/2} = 24.99$min). Since this peak was also appeared in the foreground spectrum, the yield of this peak was subtracted after extrapolation to 0 minute.

The other possible background is a Compton continuous spectrum by high energy γ rays from the activated nuclei. It was estimated by the peak-to-Compton ratio of the detector and the peak yields of the γ rays of RUN-A. The continuous background from Compton continuum was shown to be less than 10% of the event rate in the region of interest.

A low energy spectrum only due to neutron elastic scattering is shown in Fig.2.4. Here the component of other background due to the irradiation of neutron was carefully subtracted.

The light output response was obtained by comparing the experimental data and the estimated energy spectrum calculated by the Monte Carlo simulation. The angular distribution of the elastic cross section was taken into account. The experimental data [33][34] of the differential cross section of elastic scattering can be fitted by the Legendre polynomial as,

$$\frac{d\sigma}{d\Omega} = \sum_l B_l P_l(\cos\theta). \tag{2.2}$$

The fit was performed by the first five terms.

The expected energy spectrum of recoil I nuclei can be estimated by performing the Monte Carlo simulation with $f_{\rm I} = 0.05$. The recoil I events are expected to lie below 20keV.

The spectra of recoil energy of neutron elastic scattering from ^{252}Cf neutron source are expressed by the function

$$g(E_R) = \exp(p_1 E_R^3 + p_2 E_R^2 + p_3 E_R + p_4). \tag{2.3}$$

The measured energy spectrum of Fig.2.4 was fitted by the function

$$Y(E_o) = \sum_k \alpha_k g_k(E_o/f_k) + \beta(E_o), \tag{2.4}$$

where $\beta(E_o)$ is the energy function of unknown background and k stands for Na and I. E_o is the observed energy as defined in eq.(2.1).

The parameters α_k and p_4 depend on the energy threshold and the ratio of the total cross sections between Na-neutron scattering and I-neutron scattering. The ratio of these parameters were estimated by Monte Carlo simulation with the known parameters of the total cross section [35] and the energy threshold. The validity of the ratio of events were certified for each analysis.

The background spectrum, $\beta(E_o)$, was assumed to have constant value because the main component of the continuous background is the Compton scattering spectrum of high energy γ rays. The $\beta(E_o)$ was parametrized in the fitting function and forced to have positive value. Further, both the cases that the continuous background decrease and increase with the energy E_o were also analyzed. The value of $f_{\rm Na}$ was changed by the shape of the background. This effect was included in the systematic error.

From the fit, the values $f_{\rm Na} = 0.4 \pm 0.2$, $f_{\rm I} = 0.05 \pm 0.02$, and $\beta(E) \simeq 0$ in the energy region of E_0=2keV$\sim$40keV as shown in Fig.2.4. Here the quoted errors of factors f are mainly due to the systematic errors in the fitting procedure. Statistical

errors negligibly small. The systematic errors (σ_f) are estimated by using the relationship of $\sigma_f^2 = 2/(\partial^2\chi^2/\partial^2 f^2)$ in the curve fitting procedure, where χ^2 is known in the least squares method. The measured factors, f_{Na} and f_{I} are valid only the region of E_R =5keV$\sim$100keV (E_0 =2keV$\sim$40keV) and E_R =40keV$\sim$300keV (E_0 =2keV$\sim$20keV), respectively. The measured factor f_{Na} is consistent with the recent precise measurement by the Saclay group [36] [37].

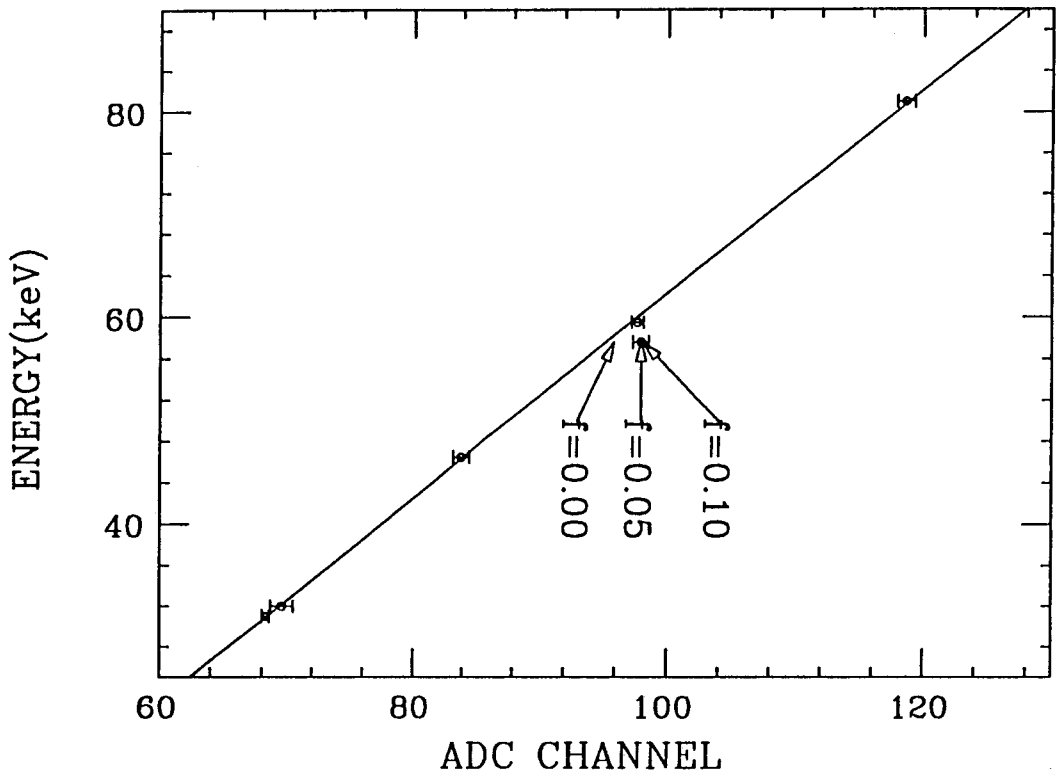

Figure 2.1: The relationship of ADC channel to energy which was measured with NaI(Tl).
closed circles The peak position which was measured by photons. The peak positions are computed by gaussian fitting. The error bars correspond the error of the fit. The linearity of calibration was quite good (correlation coefficient $r = 0.9999$). The line was computed using a least squares program.
open circle The peak position of the excited state (57.6keV).
It can be easily seen that the open circle shifts to higher energy side.

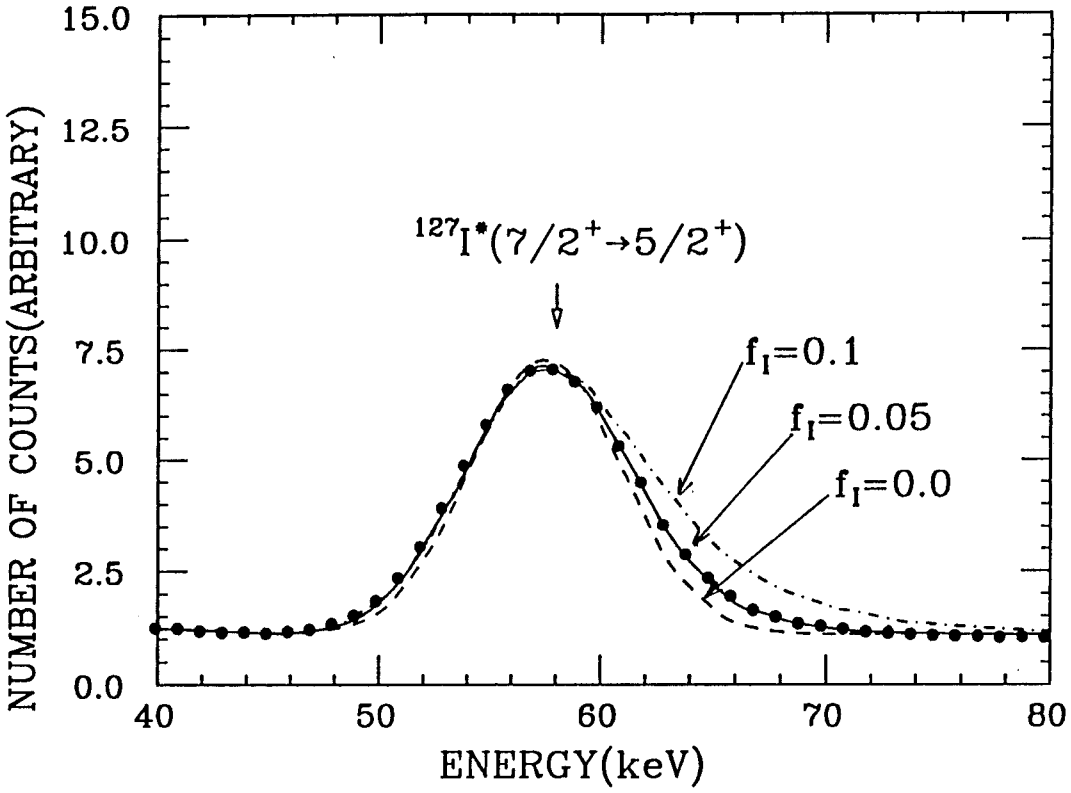

Figure 2.2: A part of the observed energy spectrum at the 50-60keV region for neutrons from ^{252}Cf. The peak corresponds to the 57.6keV γ ray from the first excited state in ^{127}I by inelastic scattering of the neutrons. The tail at the high energy side indicates the contribution from the recoil of ^{127}I. The dots show the experimental result. The solid line shows the estimated spectrum by the Monte Carlo simulation with the conversion factor $f = 0.05$. Dashed and dotted lines indicate those with $f = 0$ and $f = 0.1$, respectively, for comparison.

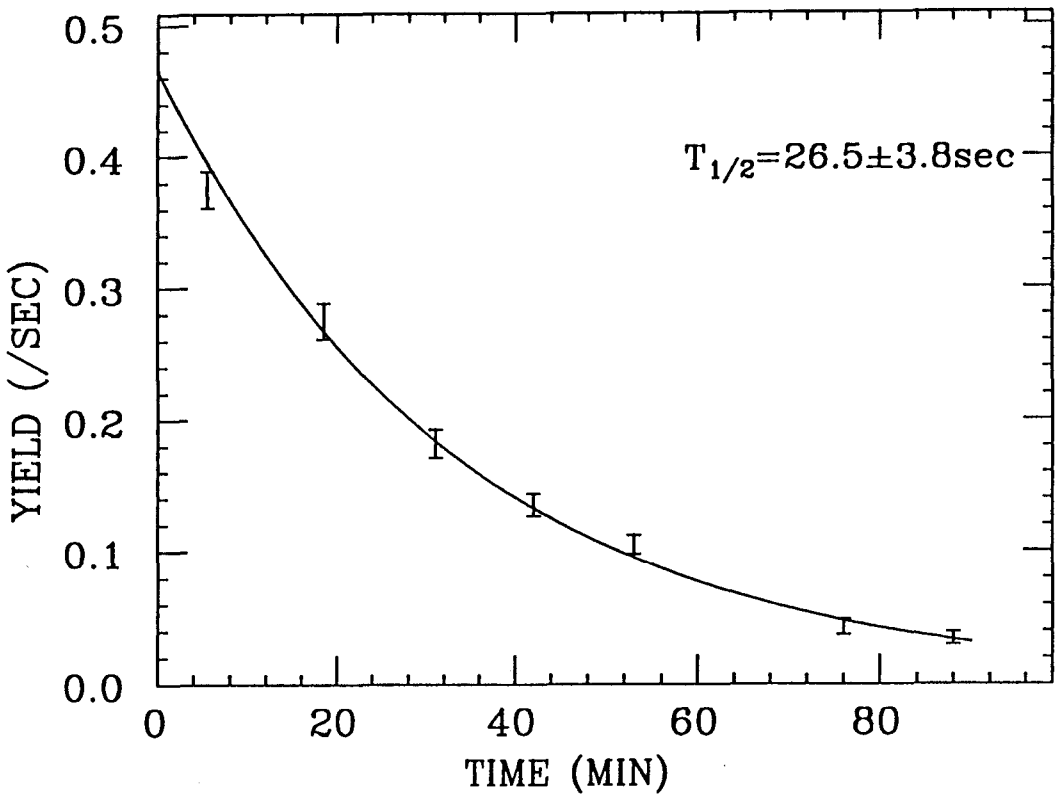

Figure 2.3: The time-intensity relation of the 28keV X ray. The half life, 26.5 ± 3.8min, is consistent with the half life of ^{128}I ($T_{1/2}$ = 25min).

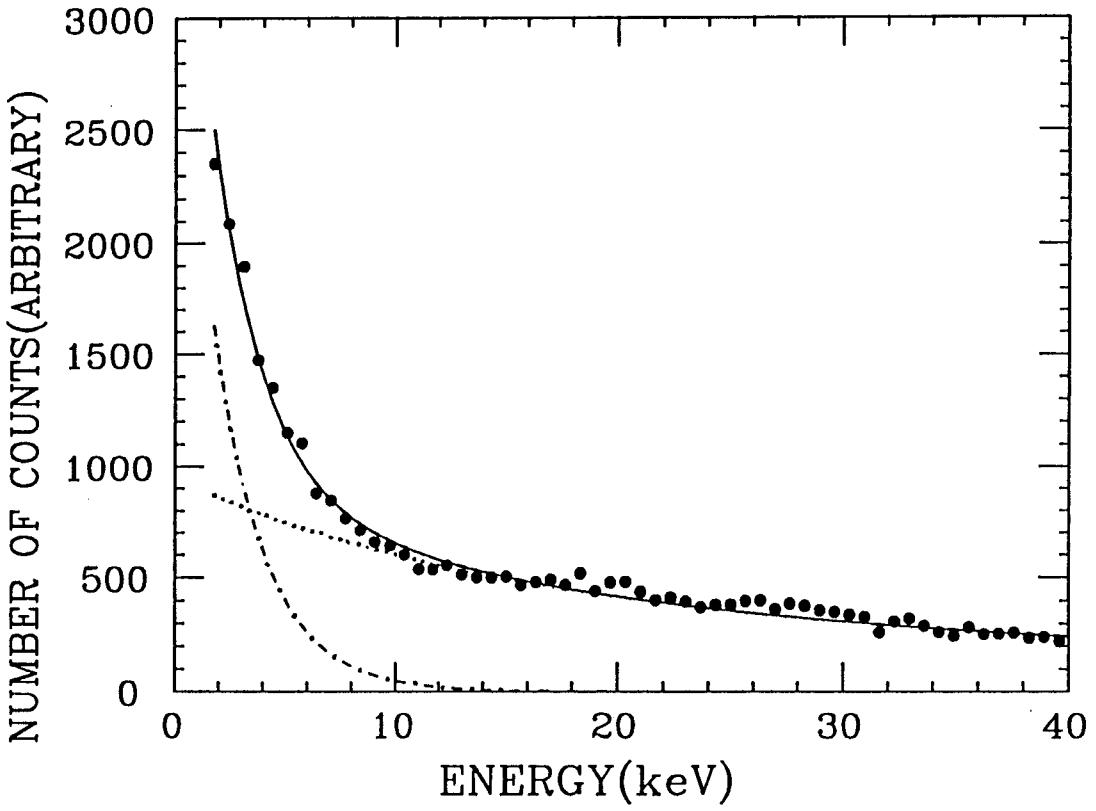

Figure 2.4: The observed energy spectrum at the 0-40keV region for elastic scattering of the ^{252}Cf neutron. All the apparent peaks were subtracted (see text). The dotted and dash-dotted lines indicate the component of ^{127}I and ^{23}Na recoil, respectively.

Chapter 3

Search for WIMPs by large NaI(Tl) scintillators

3.1 Outline of ELEGANTS V

Experimental studies of the nuclear rare processes require high sensitivity (selective) detectors with a large source. Acceptance and efficiency of the detector for the true rare events have to be large. On the other hand, huge backgrounds of natural radioactivities and of cosmic rays in the low energy region have to be rejected by hardware and/or software. The detector components themselves have to be quite free from natural radioactive isotopes.

The ultra-low-background high sensitivity detector ELEGANTS V (ELEctron GAmma-ray NeuTrino Spectrometer) has been developed at Osaka University in order to study primarily the rare $0\nu\beta\beta$ and $2\nu\beta\beta$ processes. This detector system consists of a pairs of drift chambers, 16 modules of plastic scintillators and 20 modules of NaI(Tl) scintillators and thin films of double beta decay source. Details of this system are given elsewhere [38] [39].

In order to avoid cosmic-ray backgrounds, the whole system is set at the Kamioka underground laboratory with 2700 mwe. The whole detector system is surrounded by 10cm thick OFHC (Oxygen Free High Conductive copper) bricks and 15cm thick lead bricks. External γ rays due to U and Th chain and ^{40}K from

the rock are reduced to 10^{-3} by this shield. OFHC and lead have been tested for contamination of natural radioactivities. The amounts of U and Th chain isotopes are less than a few ppb [40].

Pure nitrogen gas evaporated from liquid nitrogen is introduced into the air tight in order to replace the air containing natural Rn gas. The ^{222}Rn produces the high energy γ ray and X rays (80keV), which causes one of the serious background even in the low energy region. This effect was clearly seen in the yield of X rays of U-chain activities, which depended on the condition of the nitrogen flow. The Rn gas density in the underground laboratory is roughly 15 times higher than that in the sea level laboratory. This nitrogen circulation reduces the background level to 10^{-1}, especially it is quite effective for the reduction of the effect of X rays from U-chain activities.

The large volume NaI(Tl) scintillators were applied to search for WIMPs. For the experiment of searching for WIMPs by elastic scattering, the detector system was made of nine NaI modules out of 20 ones used for ELEGANTS V, each with dimensions of 102mm×102mm×1016mm. The experimental system is shown in Fig.3.1 For the experiment of searching for WIMPs by inelastic scattering, 20 modules of NaI were used as shown in fig.3.4.

The NaI(Tl) crystals are POLYSCIN^{TM} produced by Harshaw Co. Ltd. , each with dimensions of 102mm × 102mm × 1016mm. In general, a NaI crystal contains 1ppm potassium and ^{40}K may suffers the low energy background. The NaI crystal used for ELEGANTS V has been examined and purified to the level below 0.3ppm for potassium. The scintillator is covered with a low-background high-purity (99.999%) aluminum (Al) plate 0.8mm in thickness. The U and Th contaminations are examined to be less than 1ppb. It should be noted that normal Al case contains 10-0.1ppm U and Th isotopes.

Each NaI module is viewed at both ends by low-background 8.9cmϕ PMT.

Here K-free glass is used as the window of the PMT. A light guide of 10.2 $\times$10.2 $\times$10.2cm^3 quartz is inserted between the NaI and the PMT in order to reduce possible β and γ rays from PMT by a factor around 40.

The energy calibration and the energy resolution were obtained by using standard γ ray sources. The energy resolution for narrow beam, where γ ray sources are set at the center of the NaI(Tl) scintillator, is shown in table 3.1. It is around 20% for ^{241}Am 59.5keV γ rays, which is quite good for this type of very long NaI(Tl) detector.

Table 3.1: Energy resolution of γ and X ray measured by large NaI(Tl) of ELEGANTS V. The energy resolution are represented in FWHM.

Source	Energy (keV)	ΔE (keV)
^{57}Co	14.4	6.2
^{127}I	28	11.7
^{241}Am	59.5	12.1
^{57}Co	122	17.6

The pulse height of the PMT at one end of the NaI crystal depends on the position of scintillation with respect to the edge of the crystal. Thus one may define the roll off ratio as

$$R = \frac{V_L - V_R}{V_L + V_R}, \tag{3.1}$$

where V_L and V_R are the pulse heights of the PMTs at the left and right ends of the crystal, respectively. Here $V_L + V_R$, which gives the γ ray energy, is constant within 1% over the whole region of NaI. Consequently the energy resolution for wide beam, where γ rays enter uniformly along the long axis of NaI, remains as good as that for narrow beam. The position resolution at which γ rays hit (enter) the crystal is determined from R with a position resolution around 25cm [38]. To measure the position where a γ ray enters is useful to study the origin of the background.

3.2 Merits of NaI(Tl) scintillator

The NaI scintillator has the following advantages in searching for WIMPs.

1. **Easy to operate**

   The NaI(Tl) scintillator can be operated in room temperature. On the other hand, the Ge and Si detectors must be cooled by liquid nitrogen, and the cryogenic calorimeters and phonon detectors must to be operated in the temperature below a few tens mK!

2. **Large cross section**

   First, the ^{127}I nucleus has 74 neutrons. Thus, the matrix element for vector-coupling is as large as $g_V^2 = \left\{N_{\rm n} - (1 - 4\sin^2\theta_W)N_{\rm p}\right\}^2 = 4749$, while $g_V^2 = 1515$ for ^{74}Ge. Second, all the nuclei in the NaI scintillator have finite spin, ^{23}Na$(3/2^+)$ and ^{127}I$(5/2^+)$. Thus the spin-coupled scattering cross section is much larger than that of natural Ge detector. The abundance of ^{73}Ge $(9/2^+)$ in natural Ge detector is only 7.8%.

3. **Large volume**

   A large volume detector with a few tens of kg can be prepared easily. It makes the event rate of WIMPs nucleus scattering large and get quite good statistical accuracy. While the semiconductor can be operated with a few kg crystal and cryogenic detector can be operated with only a few tens g crystal.

In the present study, the 20 NaI detectors of the large acceptance with the mass of 36.5kg/module were applied to search for WIMPs.

However, it has a serious disadvantage in that the light output in the NaI(Tl) scintillator is reduced by factors $f = 0.4$ and 0.05 for recoiling Na and I ions, respectively, as discussed in the previous chapter. Consequently the energy region of the low momentum transfer q is likely to be hidden in the low energy noise of a

few keV. The low energy region of practical use, $E_e = 5 - 10\text{keV}$, corresponds to the ^{127}I recoil energy of $E_R \approx E_e/f = 100 \sim 200\text{keV}$, and to the large momentum transfer of $q \approx 150 \sim 200\text{MeV}/c$. Then the scattering cross-section is suppressed by the form-factor of $F(q) \sim 10^{-2} \sim 10^{-3}$.

3.3 Search for WIMPs by elastic scattering

3.3.1 Experiment

In the present experiment, the detector system was made of nine NaI modules out of 20 ones used for ELEGANTS V, each with dimensions of 102mm × 102mm × 1016mm. They are assembled as shown in Fig.3.1. The central NaI module acts as the DM detector and the surrounding 8 NaI modules act as passive and active shields.

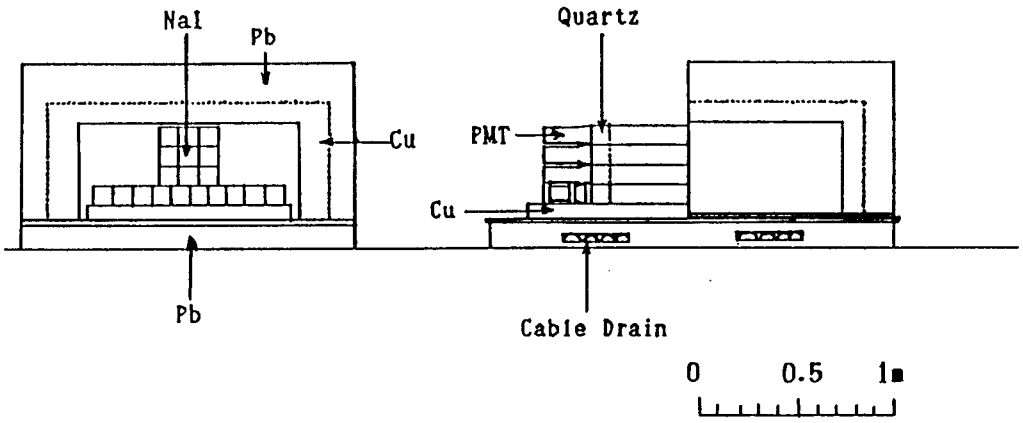

Figure 3.1: Schematic drawings of the NaI(Tl) detector arrangement in ELEGANTS V.

The pure N_2 gas evaporated from the liquid nitrogen was introduced into the air tight to replace the air containing natural Rn gas. The 5cm thick acrylic plates

and small the air bags filled with pure N_2 gas were placed on the NaI(Tl) detectors in order to keep the air away from the detectors.

The pulse height spectrum of the central NaI detector in anticoincidence with all pulses from the surrounding 8 NaI detectors were observed. The energy scale is calibrated by using the 59.5keV and 17.5keV γ-ray and X-ray from ^{241}Am source, 14.4keV and 122keV γ-rays from ^{57}Co source and 28keV X-ray from ^{127}I in NaI detector itself.

The energy signal was converted into digital channel data by the charge ADC (LeCroy 2249W). The energy scale is calibrated by using the 59.5keV and 17.5keV γ-ray and X-ray from ^{241}Am source, 14.4keV and 122keV γ-rays from ^{57}Co source and 28keV X-ray from ^{127}I in NaI detector itself. All the pulse height data from all the NaI modules were stored into the 1GB hard disk in PDP-11/53. These data were copied to magnetic tapes and analyzed by FACOM M360 computer system in Osaka University.

3.3.2 Analysis and limit on the WIMPs

The typical low part of the observed spectrum is shown in Fig.3.2 for a live time of 6.0days (220kg·day).

The bump at the 46.5keV is due to extremely small amount ($\sim 2.6\times10^{-3}$ Bq/kg) of ^{210}Pb radioactive contamination inside the NaI crystal [39]. The low energy β ray (Q_β = 64keV) and following beta decay of ^{210}Po (Q_β = 1160keV) suffer the background rate below a few tens keV (see Fig.3.3). The contribution of β rays from ^{210}Pb decay in the low-energy region ($\sim$ 10keV) spectrum was estimated by the Monte Carlo simulation based on the observed peak yield of the 46.5keV γ ray from ^{210}Pb. The estimated fraction of the event rate at the threshold energy was 2.9count/keV/day/kg. The noise threshold is around 4keV and the unknown background rate at 5keV is around 5.1/keV/day/kg as shown in Fig.3.2, which are

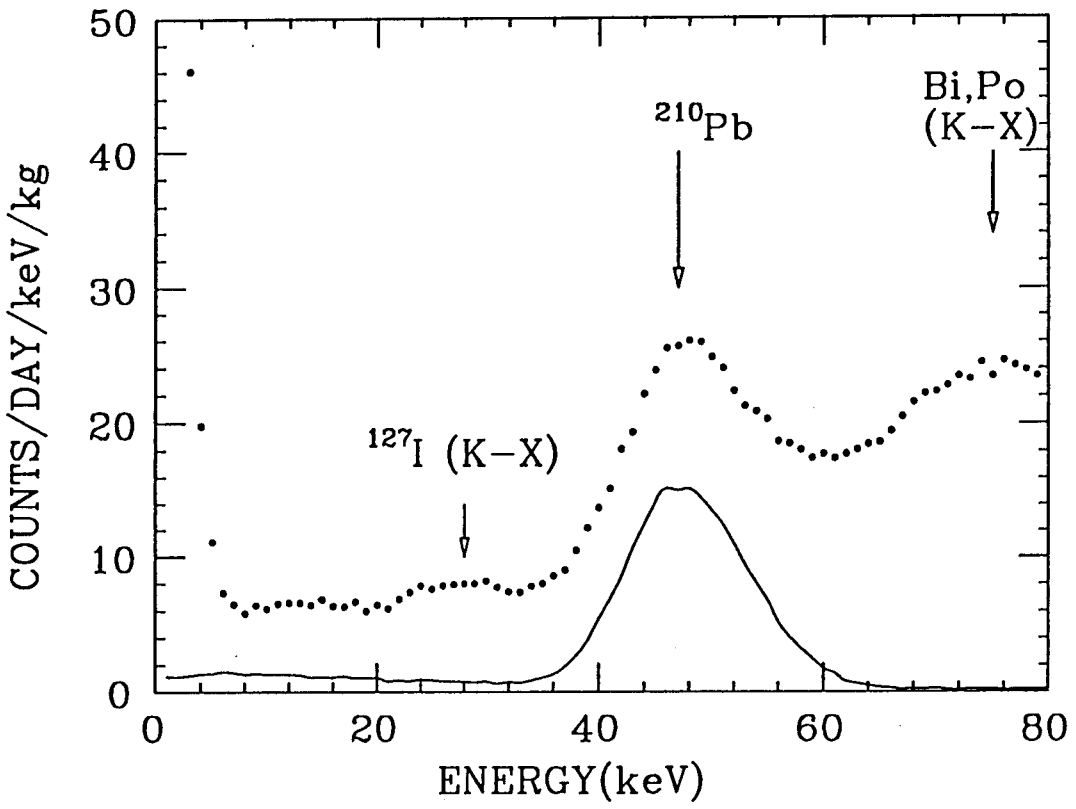

Figure 3.2: Observed spectrum at the energy region of the present interest. The closed circle was the experimental result. The solid line shows the estimated energy spectrum of gamma and beta rays from the decay chain ^{210}Pb-($\beta\gamma$)$\rightarrow$^{210}Bi-(β)$\rightarrow$^{210}Po.

remarkably low levels for this type of large NaI detector.

Evaluating the limit on the maximum halo density of the DMs, the observed spectrum, shown in Fig.3.2, was analyzed in terms of the recoil spectra of ^{23}Na and ^{127}I with the measured output responses. The small value of the output response ($f_{\rm I}$) affects the lowest measurable energy of ^{127}I recoil. The threshold energy of E_0=5keV corresponds to E_R=100 keV, and the condition of $qR \ll 1$ is broken. We must consider the finite size effect of the nucleus in the DM-nucleus cross section. The finite size effect of the cross section is written in terms of a form factor $F(q)$

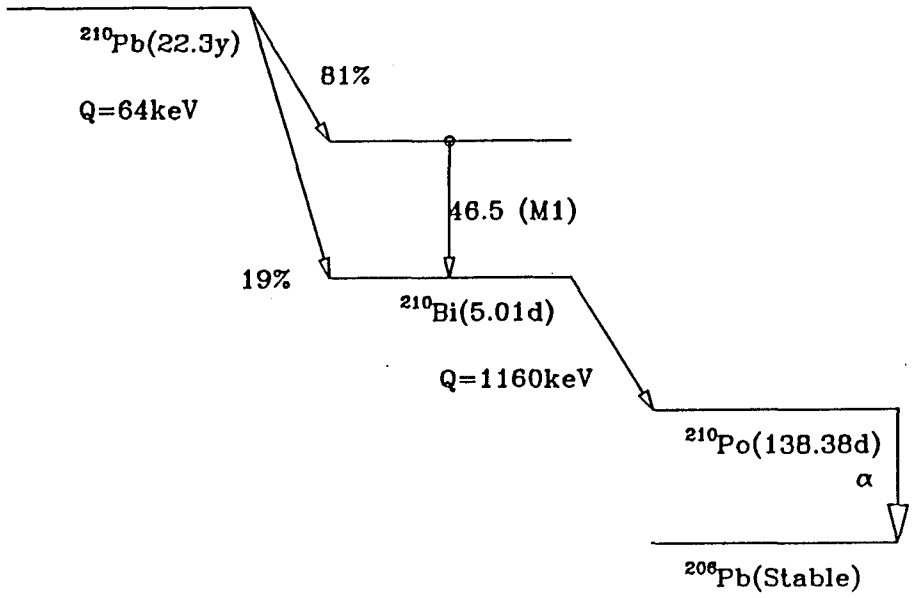

Figure 3.3: Decay chain and level scheme of ^{210}Pb$\rightarrow^{210}$Bi $\rightarrow^{210}$Po $\rightarrow^{206}$Pb [41].

as

$$\frac{d\sigma}{d\Omega} = (\frac{d\sigma}{d\Omega})_{point}|F(q)|^2, \tag{3.2}$$

where $(d\sigma/d\Omega)_{point}$ is the cross section of the DM-nucleus elastic scattering by using g_V and g_A in eq.(1.8) and eq.(1.9), which are calculated assuming that the target nucleus is a point particle.

In the case of ^{127}I, since the threshold energy of $E_0 = 5$keV ($E_R = 100$keV) corresponds to the momentum transfer $q \sim 0.8\text{fm}^{-1}$, the form factor $|F(q)|^2$ ($= |\int \rho(r)\exp(-iqr)d^3r|^2$) is about 0.02, where $\rho(r)$ is the nucleon density in the nucleus. Thus the limits on DM is weaker by a factor 1/50 than that assuming the point target nucleus.

The evaluated maximum halo density limits on ν_D and ν_M are shown as solid lines in Fig.3.6. The upper dotted curve shows the exclusion continuum for the local density of Majorana neutrino, and the lower dashed one shows that for Dirac neutrino. The upper area of the curves shows the excluded area for the density of each particles as a dark matter. The bend in the line for ν_D in the mass region lower than 30GeV is due to the effect of ^{23}Na. Since ^{23}Na is as 1/4 massive as ^{127}I, the event rate per keV of the mass range below 30GeV by ^{23}Na recoil is larger than that by ^{127}I recoil.

Since ^{127}I has much more neutrons than ^{23}Na , it gives more stringent limit on the density of ν_D than ^{23}Na although the form factor of ^{127}I is much smaller. On the other hand, ^{23}Na with the form factor $|F(q)|^2$ $(=|\int |\psi_{nl}(r)|^2 \exp(iqr) d^3r|^2) \simeq 1$ gives more stringent limit on the density of ν_M than ^{127}I, where $\psi_{nl}(r)$ is the wave function of the valence nucleon carrying the spin. These limits are weaker than Ge experiment [23] by a factor of 5 for ν_M and a factor of 100 for ν_D. For the other particle candidates, the curves move by the factor of N_k listed in table 1.2.

3.4 Search for spin-coupled WIMPs by inelastic scattering

This section reports the first study of spin-coupled WIMPs by direct measurement of axial-vector (inelastic spin) excitation of nuclei in a large-volume scintillator [43].

The present work is concerned with direct measurements of DM by observing the interaction of DM with nuclei in detectors. Direct measurements of DM, however, are very hard because of the small DM density ρ_D, the weak interaction (coupling) strength and of the low energy signal. So far, direct measurements have been made mostly by observing the nuclear recoil energy induced by the elastic scattering of DM[1]. The candidate particle mass, m_χ, is of the order of GeV-TeV, while the DM velocity (v_i) with respect to the Earth is of the order of $v_i \approx 10^{-3}c$ with c being the velocity of light. Consequently the recoil energy E_R is as small as $E_R = 10 \sim 100$keV.

Merits of the NaI detector are the large volume, the low background rate, and the 100% abundance of the finite-spin nuclei of ^{23}Na and ^{127}I in the detector. It has, however, a serious demerit that the light-output in the NaI(Tl) scintillator is reduced by factors $f = 0.4$ and 0.05 for recoil Na and I ions, respectively [29]. Here f is defined as the ratio of the light response (E_e) for electrons (γ rays) to that (E_R) for ions. Consequently the energy region of the low momentum transfer q is likely to be hidden in the low energy noise of a few keV. The low energy region of practical use, $E_e = 5 - 10$keV, corresponds to the ^{127}I recoil energy of $E_R \approx E_e/f = 100 \sim 200$keV, and to the large momentum transfer of $q \approx 150 \sim 200$MeV/c. Then the scattering cross-section is suppressed by the form-factor of $F(q) \sim 10^{-2} \sim 10^{-3}$. Furthermore the absolute cross-section itself is uncertain because the nuclear spin matrix element is not known experimentally

and cannot be evaluated theoretically with reasonable accuracy.

The key point of the present study of the inelastic scattering of DM is to avoid these demerits, still keeping the major advantages of the scintillator. The light output is the sum of E^* for the γ-decay and fE_R for the recoil energy. Therefore the energy region to be looked for in the inelastic process is shifted to the higher energy region around E^* from the very low energy region of $fE_R \sim$ a few keV in the elastic scattering case. There, the DM signal can be fairly free from the low energy noise in the few keV region. Consequently scattering involving low momentum transfer, with the form factor $F(q) \approx 1$, can be investigated. It is important to note that the spin matrix element for the inelastic scattering is known(or evaluated) from the inverse process of the M1 (magnetic dipole) γ deexcitation as shown in the previous work [46].

The differential cross-section for the inelastic scattering of the spin-coupled DM from a nucleus of mass m_N is expressed as

$$\frac{d^2\sigma}{dp_i d\Omega} = N_k(\frac{m_N \cdot m_\chi}{m_N + m_\chi})^2 \cdot G_F^2 g_A^2 F^2(q) \frac{p_f}{p_i} f(p_i) \frac{1}{4\pi}, \tag{3.3}$$

where p_f/p_i is the phase-space factor with p_i and p_f being the momenta of the incident and outgoing (scattered) DM, Ω is the solid angle for the scattered DM, $f(p_i)$ is the DM momentum distribution and N_k is the constant for the k-type DM shown in table 1.2. The momentum distribution is assumed to be Maxwellian distribution with the average velocity being $\beta = v_{DM}/c = 10^{-3}$ and the maximum velocity being $\beta = 1.8 \times 10^{-3}$.

The momentum transfer q is related to the recoil energy as $q^2/2m_N = E_R$. The energy and the momentum conservation are given as $p_i^2/2m_\chi = p_f^2/2m_\chi + E^* + E_R$ and $p_i = p_f + q$, respectively.

The event rate of the inelastic scattering at the solid angle Ω is expressed as

$$\frac{ds}{d\Omega} = \rho_T \rho_D \int \frac{d^2\sigma}{dp_i d\Omega} v_i dp_i, \tag{3.4}$$

where ρ_T is the nuclear number density of the target (detector) and $\rho_D(= 0.3\text{GeV})$ is the local DM density near the earth. For given incident momentum P_i, the recoil momentum q and the recoil energy E_R are related uniquely to the scattering angle Ω. The recoil energy E_R is converted to the light out-put (pulse-height) of the scintillator as $E = E^* + fE_R$. Consequently the recoil energy spectrum $S(E_R)$ is deduced from eq.(3.4) as $S(E_R) = (ds/d\Omega)(d\Omega/dE_R)$. Then the output (pulse-height) spectrum $S(E)$ is obtained by using the relation of $E = E^* + fE_R$.

In fact the pulse-height spectrum (event rate) is concentrated at $E \approx E^*$ because of the small f factor ($f \leq 0.05$) and of the small form factor $F(q)$ at large E_R (i.e. at large q).

The inelastic scattering from ^{127}I in the NaI detector was studied in the present work. The low lying $7/2^+$ state at 57.6keV and the $3/2^+$ state at 202.8keV can be excited by the inelastic scattering of the spin coupled DM. The spin matrix elements λ_N are evaluated from the known γ transition rates for these states[41].

The experimental data were taken from the one in the previous work concerning with the exotic K X-rays from iodine atoms [46]. The experiment was carried out with 20 modules of 10.2cm×10.2cm×101.6cm NaI(Tl) scintillators of ELEGANTS V system as shown in Fig.3.4.

The inelastic scattering process is followed mostly by the single M1 γ-ray. Thus data were taken by recording the single-hit event from any one NaI crystal among 20 modules in anticoincidence with the other 19 modules. Energy spectra, for the live time of 1818 hours, from 17 of the NaI modules were summed for the final energy spectrum; other 3 NaI modules were not sufficiently free from radioactive impurities.

The observed spectrum, as shown in Fig.3.5 (a), indicates no distinct peaks at either $E^* = 57.6$keV or $E^* = 202.8$keV. Here we confine our attention to the excitation of the 57.6keV excited state because both the spin matrix element and

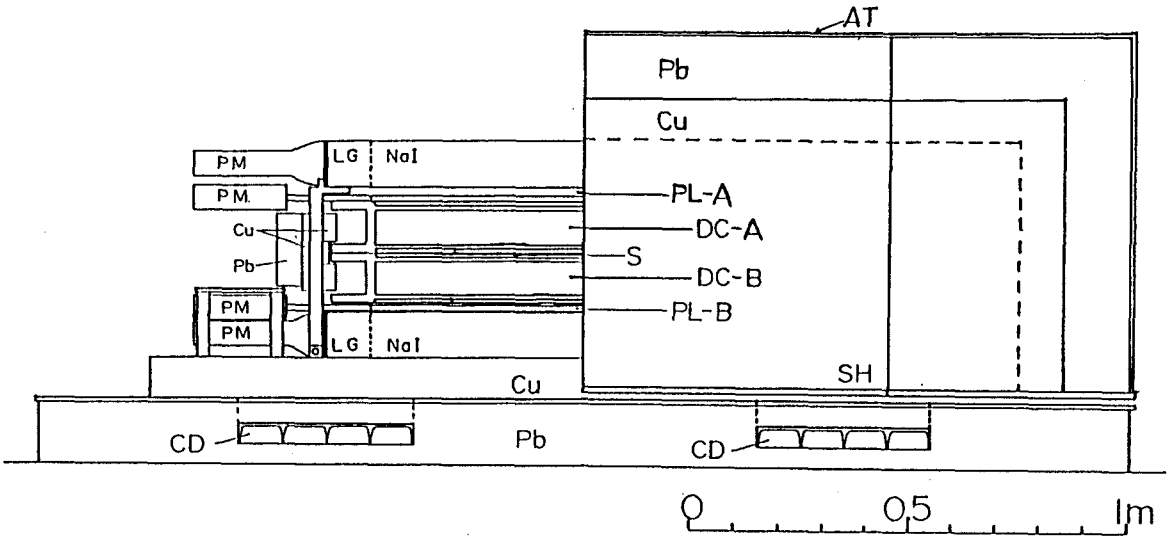

Figure 3.4: Schematic side view of ELEGANTS V, where the left-side part of the movable shield is opened to show the detectors inside the shield box. SH: movable shield, Pb: lead bricks, Cu: OFHC copper bricks, NaI: NaI detector array, LG: light guide, PM: photomultiplier, PL-A and PL-B: plastic scintillators, DC-A and DC-B: drift chambers, S: source plane, CD: cable duct and AT: air tight container.

the fraction of the DM flux contributing to the excitation are larger than those for the 202.8keV state (note that the $E^* = 202.8$keV is so high that only the higher energy components of the DM velocity distribution can contribute to exciting this state).

The observed pulse height spectrum can be composed of the following background components.

1. β ray from ^{210}Pb to the ground state of ^{210}Bi($Q_\beta = 63$keV).

2. β ray from ^{210}Pb to the excited state at 46.5keV of ^{210}Bi(Q_β =16.5keV).

3. γ ray from the excited state of ^{210}Bi(46.5keV).

4. X rays from U-chain.

5. Continuous background.

Almost all the ^{210}Pb was found to be contained in the NaI(Tl) crystal because of the following reasons.

(a) The event rate of this peak did not depend on the other backgrounds. The event rates of the peaks of the X ray at 80keV and γ rays are continuously monitored. These event rates depended clearly on the condition of the nitrogen flow. However, the event rate of 46.5keV γ ray did not depend on the background rate.

(b) The 46.5keV peak could not be reproduced only by single gaussian peak.

Since the half-life of ^{210}Pb (22.3y) is much longer than the measurement time, the effect of the Rn gas to the yield of the 46.5keV γ ray is much smaller than the statistic and systematic errors.

The spectrum was analyzed by means of the least-square fit with these background components. The fitting function was folded with the observed energy resolution given by $\Delta E = 7.8 + E/12$ keV (FWHM). The observed spectrum was reproduced by the fit, without introducing the finite yield of the inelastic excitation by WIMPs. Fig.3.5(b) shows the difference between the observed spectrum and the least square fit without introducing the inelastic excitation by WIMPs.

The upper limit of the yield of the γ ray from the inelastic excitation was derived from the spectrum by least square fit with the gaussian peak of the γ-ray and the deviation of the previous fit. The energy resolution was also given by

the experimental data as $\Delta E = 7.8 + E/12 = 12.6$keV (FWHM). The effect of the recoil energy was not taken into account because of the small value of f, form factor and large energy resolution. Especially, kinetic energy of WIMPs are limited by the escape velocity of the galaxy, $E_{\max} = m_\chi \beta_{575}^2/2$, where β_{575} is the escape velocity of the galaxy. Consequently, neither peak shift or a tail cannot be seen. The upper limit of the WIMPs inelastic scattering deduced from the χ^2 test of the fit is $s \leq 9.8 \cdot 10^{-2}$ counts/day/kg (2σ). The solid line in Fig.3.5(b) shows the possible spectrum of the DM inelastic scattering at 2σ C.L.

Using this upper limit of the event rate, one gets the limit on the local density ρ_D of the certain DM candidates. The exclusion plot is shown in Fig.3.6. Since the DM needs to have enough energy to excite the ^{127}I, the present method is not sensitive over the lower mass range , but is very useful for heavier mass DM.

It should be emphasized that the present limit for the spin-coupled DM is severer than the previous one derived from the elastic scattering (see Fig.3.6), and that the present one is based on the observed matrix element for the inelastic excitation while the previous one on the theoretically estimated one for the elastic process.

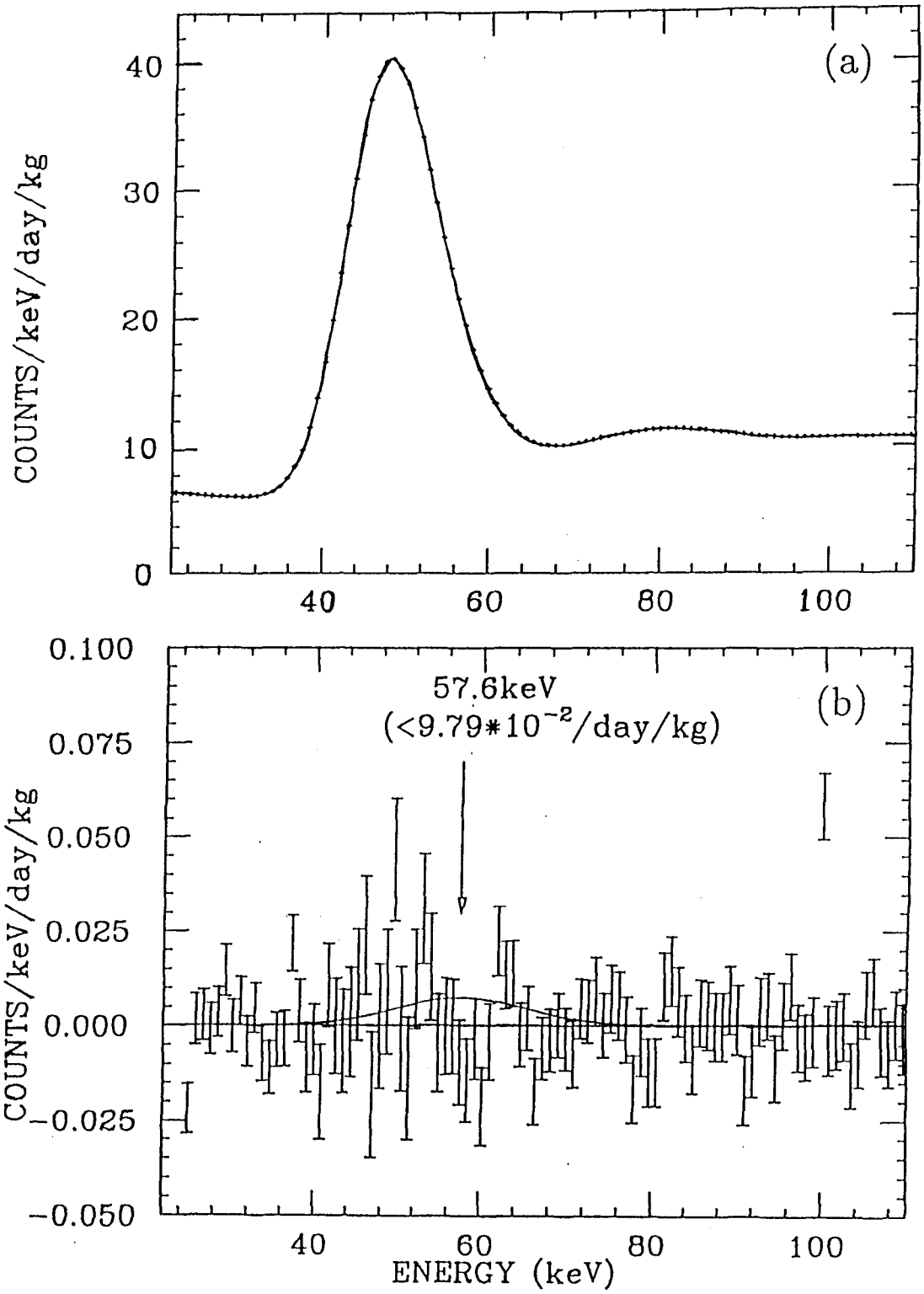

Figure 3.5: (a) The observed energy spectrum in the low energy region for the live time of 1818 hours. The solid line is the least square fit (see text).
(b) The subtracted spectrum of the 17 NaI scintillator [39]. The gaussian peak shows the possible spectrum of the inelastic scattering with the given event rate, corresponding to the 2σ limit.

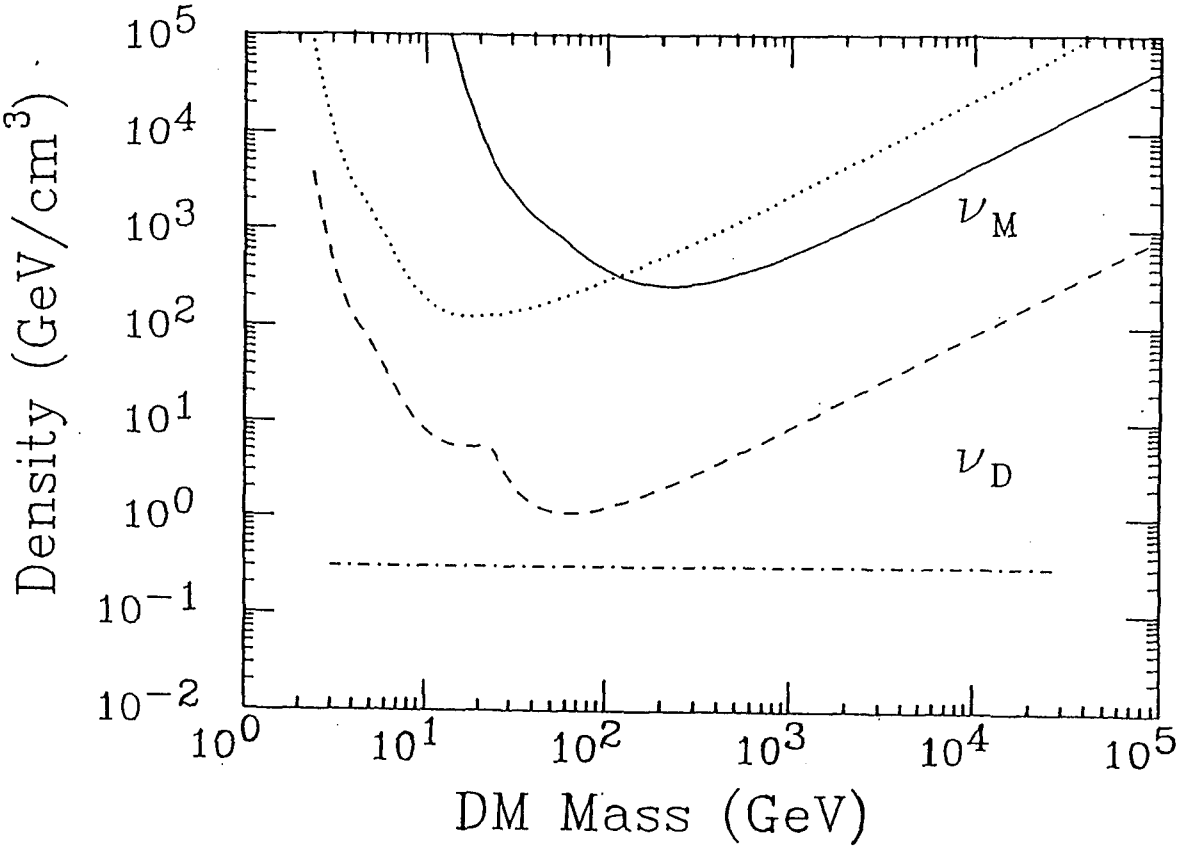

Figure 3.6: The exclusion plot with the 90% confidence level for the density of the Dirac neutrino (lower) and the Majorana neutrino (upper). The solid line indicates the present limit on the local density of the Majorana neutrino. The dotted and dashed lines are the limits derived from elastic scattering for the Majorana ν and the Dirac ν, respectively. Upper regions from the lines are excluded. The dash-dotted line indicates the critical density of 0.3GeV/cm^3.

Chapter 4

Discussions and perspectives

4.1 Discussion of NaI(Tl) scintillator as a WIMPs detector

The large NaI detectors of ELEGANTS V have been applied to search for WIMPs. A NaI(Tl) detector is shown to have great advantages of a large nuclear matrix elements, g_V and g_A, and 100% abundance of odd-A nuclei. In the previous work, a low noise ($\simeq$ 5keV) and low background ($\simeq$ 8/day/keV/kg) were achieved by a huge (36.5kg/module) NaI(Tl) detector. The elastic scattering and inelastic scattering of WIMPs were studied and the strong limits on the density of WIMPs were obtained. However, a NaI(Tl) is shown to have demerits of a small form factor for the WIMPs-^{127}I scattering due to a small light output for the recoil ^{127}I nucleus.

In order to set more stringent limit to exclude such candidates as a dark matter, the following properties are required.

1. **Small nuclear radius**

   In case of a NaI(Tl) scintillator, it has a serious disadvantage that the light output response is reduced by factors $f = 0.05$ and 0.4 for recoiling I and Na ions, respectively. Consequently the low energy region of practical use, $E_o = 5 - 10$keV, corresponds to the I recoil energy of $E_R = 100 \sim 200$keV,

and to the large momentum transfer of $q \simeq 150 \sim 200\mathrm{MeV}/c$. Then the scattering cross section is suppressed by the form factor.

A light nucleus, eg. ^{23}Na and ^{19}F, has a small nuclear radius enough to approximate to a point particle whenever the momentum transfer is large.

2. **Large matrix element**

   The matrix element for the elastic scattering is needed to be large. The spin matrix elements for many odd-A nuclei have been evaluated in terms of the single particle shell model and the odd-group model [47]. The spin matrix elements of the ^{23}Na and the ^{127}I nuclei have a quite large model dependence. On the other hand, the spin matrix element for the elastic scattering of the ^{19}F nucleus is large and can be well evaluated theoretically with small model dependence. The advantages of a CaF_2(Eu) will be discussed below.

From these arguments, a CaF_2(Eu) scintillator is the quite promising detector to search for spin-coupled WIMPs candidates.

4.2 Advantages of CaF_2(Eu)

A large volume CaF_2(Eu) scintillator can be applied to search for spin-coupled WIMPs candidates. Since the ^{19}F nucleus has a finite spin ($J = 1/2$), the spin matrix element of the nucleus-WIMPs elastic scattering is large. Recently, the nuclear spin matrix elements, $\lambda^2 J(J+1)$, have been evaluated in terms of the odd-group model [47]. ^{19}F has been shown to have small model dependence and large spin matrix element.

There are three fluoride scintillator materials, CaF_2(Eu), CsF and BaF_2. The low background, large mass fraction of ^{19}F and large light output are required for WIMPs search. The properties of these scintillators are listed elsewhere. The important characters of them for WIMPs search are shown below.

1. **Low background (High purity)**

   To develop a low background detector system, a high purity crystal is needed. The purity of a CaF_2 crystal is remarkably high (99.999%), because it is prepared for optical lenses. On the other hand, the BaF_2 contains a large amount of U-chain radioactivities (approx. 74Bq/kg) and the CsF contains a large amount of radioactive ^{137}Cs.

2. **Large mass fraction**

   The large mass fraction of ^{19}F nucleus is quite important property to search for spin-coupled WIMPs candidates. The mass fractions of ^{19}F in a CaF_2, a BaF_2 and a CsF are 0.49,0.22 and 0.13, respectively.

3. **Large light output**

   The energy threshold and the energy resolution depend on the light output yield. The light output yield of the CaF_2(Eu) scintillator, the BaF_2 scintillator and the CsF scintillator relative to the one of NaI(Tl) scintillator are 0.5, 0.16 and 0.06, respectively.

4. **Easy to handle and operate.**

   The easiness of handling the detectors depends on their hygroscopic property. A CaF_2(Eu) crystal and a BaF_2 crystal are not hygroscopic but a CsF crystal is. Consequently a CsF is not the best crystal from this point of view.

From these points of view, the CaF_2(Eu) crystal is the best fluoride scintillator for WIMPs search.

Comparing the CaF_2(Eu) scintillator with the NaI(Tl) scintillator, the mass fraction of ^{23}Na in NaI(Tl) is as small as 0.15. Thus the effective mass of CaF_2(Eu) is three times larger than that of NaI(Tl). The light output of NaI(Tl) is twice as large as CaF_2(Eu), however, it is not a serious demerit, because the low energy threshold below 5keV can be achieved with a CaF_2(Eu) scintillator.

The advantages of the detectors to search for the spin-coupled WIMPs can be compared by the figure of merit defined as,

$$F_M = a_N \frac{4 m_\chi m_N}{(m_\chi + m_N)^2} \frac{4}{3} \lambda^2 J(J+1). \tag{4.1}$$

where a_N is the mass fraction of a target nucleus in the detector. The figure of merits of ^{19}F, ^{127}I, ^{23}Na and ^{73}Ge in CaF_2(Eu), NaI(Tl) and Ge are listed in table 4.1. This table shows that a CaF_2(Eu) scintillator has great advantage for studying spin-coupled dark matters because of the large F_M and small ambiguity between the models. It should be noted that ^{127}I in NaI(Tl) scintillator is not a good nucleus because of its small form factor, although it has a large figure of merit.

Table 4.1: Figure of merits for ^{19}F,^{127}I, ^{23}Na and ^{73}Ge in a CaF_2(Eu) scintillator, a NaI(Tl) scintillator and a natural Ge semiconductor detectors, respectively. Both the spin matrix elements, $\lambda^2 J(J+1)$, evaluated by the single particle model and the odd-group model are shown.

Isotope	J	a_N	$F_{M(\mathrm{sing})}$	$F_{M(\mathrm{odd})}$
^{19}F	1/2	0.49	0.263	0.227
^{23}Na	3/2	0.15	0.043	0.005
^{127}I	5/2	0.85	0.280	0.008
^{73}Ge	9/2	0.078	0.031	0.007

From these properties, the CaF_2(Eu) scintillator is the most promising detector to search for spin-coupled WIMPs candidates.

4.3 Tests of the CaF_2(Eu) for spin-coupled WIMPs search

The following properties of CaF_2(Eu), which are important to search for WIMPs, were studied.

1. Light absorption
2. Light output
3. Low energy threshold
4. Light output response of alpha ray

4.3.1 The light absorption

Since CaF_2(Eu) has a sharp absorption band at 400nm which partly overlaps with the scintillation emission band, a large (long) detector system cannot be applied. However, the large detector system is needed for DM, thus the possibility of thick crystal have to be tested. The effect of the light absorption was measured the relation between the peak positions of the gamma ray and the position where it was introduced. The 60keV gamma ray from ^{241}Am was introduced through a 1cm thick OFHC collimator with a 2mmϕ hole. The distances between the noise and the peaks were 180, 176 and 168 channels, when the gamma ray was introduced into the end of the crystal where the PMT was connected, into the center of the crystal and into the other end of the crystal, respectively. Since the difference of the peak position was not so large, the decline in the number of photon does not affect so seriously. The light absorption may suffer the energy resolution, but it can be improved when the PMTs are attached at both sides of a crystal and the pulse heights are summed.

4.3.2 The light output ratio relative to NaI(Tl)

The light output of a CaF_2(Eu) relative to the light output of a NaI(Tl) was measured by the energy resolution. The energy resolution $\Delta E/E$(FWHM) of a scintillation detector is related to the energy,w, which is needed to create a scintillation photon as,

$$\frac{\Delta E}{E} = \frac{2.35\sqrt{w}}{\sqrt{E}}. \tag{4.2}$$

The inverse of w is proportional to the light output ratio. Thus the ratio of light output can be measured by measuring the energy resolution of a scintillator.

The energy resolutions at 60keV (γ ray from ^{241}Am) for a CaF_2(Eu), a CaF_2(pure) and a NaI(Tl) were measured. The energy resolution was measured by The $\Delta E/E$ (FWHM) and the light output ratio to NaI(Tl) are listed in table 4.2. Since the

Table 4.2: The energy resolutions $\Delta E/E$(FWHM) and light output ratio. The light output ratios are normalized NaI(Tl) so that the light output of NaI(Tl) is 1.

Crystal	$\Delta E/E$ (FWHM)	Light output (NaI(Tl)=1)
NaI(Tl)	13%	1.0
CaF_2(Eu)	18%	0.5
CaF_2(pure)	48%	0.07

extremely low energy measurement (below 10keV) is needed to study the elastic scattering of WIMPs, Eu dope is important. Though the CaF_2(pure) is applicable to large detector system, it cannot be used for dark matter search because of its small light output.

4.3.3 The low energy threshold

To achieve low energy threshold is quite important for DM search. The energy threshold of the CaF_2(Eu) detector was studied with low energy γ and X rays. A CaF_2(Eu) detector provided by BICRON Co. Ltd. with the dimension

of 10.4cm×10.5cm×2.54cm was used for this measurement. It was viewed by two PMTs from both ends of the crystal.

The energy threshold was determined by the extrapolation of the energy calibration. The energy calibration was obtained by using standard γ ray sources, 31keV (K-X ray from ^{133}Ba), 46.5keV (γ ray from ^{210}Pb), 59.5keV (γ ray from ^{241}Am) and 81keV (γ ray from ^{133}Ba). The L-X rays from Np (daughter of ^{241}AM) could not observed because of the absorption by the 0.8mm thick aluminum housing. The energy-ADC channel relationship shows the excellent linearity (correlation coefficient $r = 0.99998$).

A low energy spectrum is shown in Fig.4.1. It can be seen that the energy threshold is 4keV. It is quite low energy threshold to set stringent limit on the density of WIMPs.

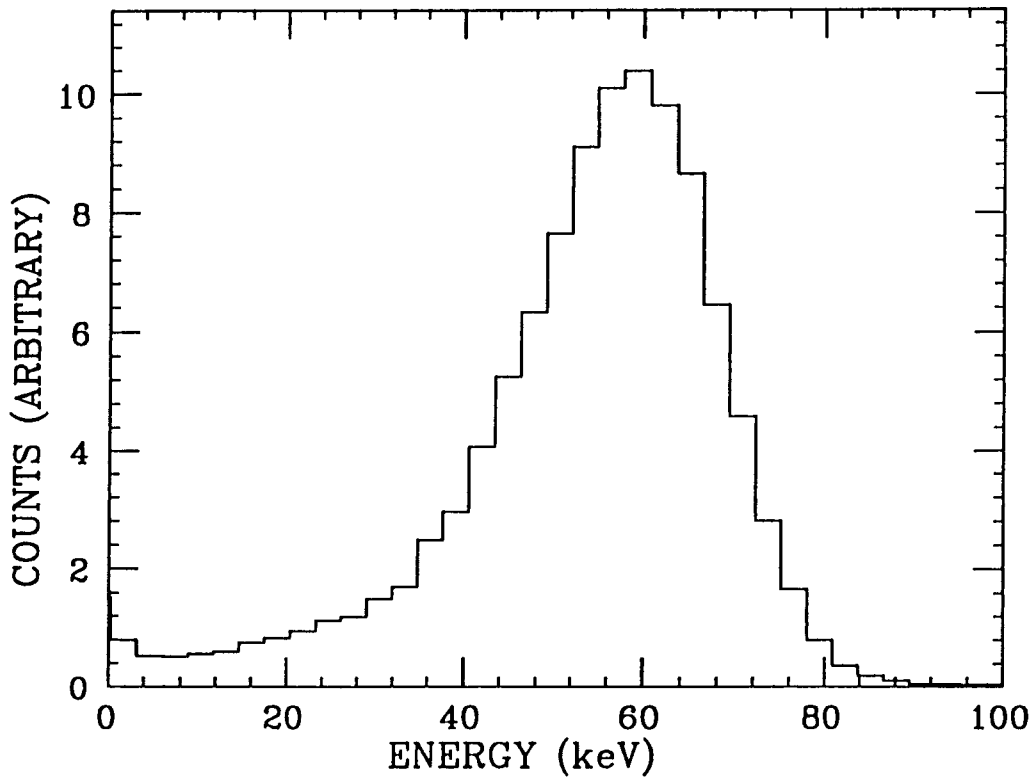

Figure 4.1: Test of low energy threshold for CaF_2(Eu) detector. The γ source is ^{241}Am (59.5keV).

4.3.4 The light output response of alpha ray

The energy spectrum of the alpha rays from the U-chain contaminants can be used for the energy calibration in the high energy region. Thus the light output response of the alpha ray is important for studying the origin of the high energy γ backgrounds. A $CaF_2(Eu)$ detector with the dimension of 2inchesϕ×2inches was used to study the alpha response. The crystal was provided by Oyo-Koken Co. Ltd. The γ rays of 511keV, 1274keV (^{22}Na) and 662keV (^{137}Cs) were used for the calibration of the energy-ADC channel relationship. Since the alpha ray stops immediately after its entrance into the crystal, the collimated gamma rays were introduced into the other end of the crystal where the PMT was connected in order to avoid the effect of the light absorption. The observed energy spectra of γ rays are shown in Fig.4.2(a). The energy resolution was fairly good because the γ rays were collimated. The alpha ray source (^{241}Am;Q_α = 5.486MeV) was also placed on the same end of the crystal.

The light output response of α ray is derived as,

$$f_\alpha = \frac{E_o}{E_\alpha}. \tag{4.3}$$

Where E_α is the kinetic energy of α rays and E_o is the electron equivalent energy. The light output and the electron equivalent energy were calibrated by three photo-peaks, 511keV, 662keV and 1274keV. Since the α rays pass through 0.7mm of air, the energy loss by the air is only 75keV. Thus the energy loss does not affect the analysis. The peak position of the alpha ray obtained as shown in Fig.4.2(b) was E_o = 958keV. It leads to the response of alpha ray as f_α = 0.17. The same result was derived by BRS group [37].

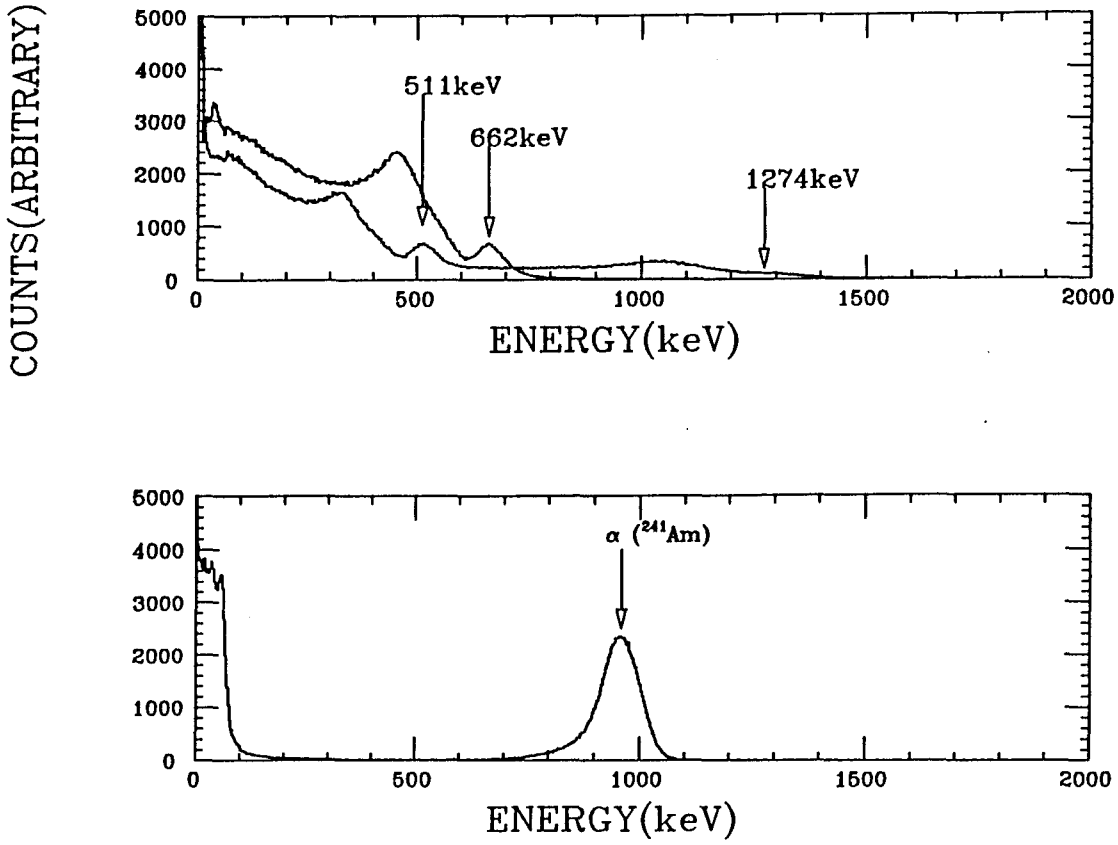

Figure 4.2: (a) The energy spectrum of calibration for energy-ADC channel measured by CaF_2(Eu). The γ source was ^{22}Na (551keV,1274keV) and ^{137}Cs (662keV). (b) The measured energy spectrum of α source (^{241}Am) with CaF_2(Eu) [41].

4.3.5 The low BG measurement of CaF_2(Eu)

The low background measurement was performed in Osaka University (sea level). The experimental system was set in a laboratory of Radio Isotope Center. A CaF_2(Eu) detector with the dimension of 5.1cmϕ×2.54cm was used. This crystal was viewed by two photo-multiplier tubes from both ends of the crystal.

This CaF_2(Eu) detector was surrounded by eight modules of NaI(Tl) scintillators of 10.2cm cube. They acted as active shields against Compton γ rays and cosmic rays.

This system was covered with 5cm thick OFHC bricks and 10cm thick lead bricks. These shields reduce the external background by a factor around 10^{-2}.

The resulting energy spectrum shows there were some prominent peaks by the

alpha rays (see Fig.4.3). They are due to the U-chain contaminants which are contained in the $CaF_2(Eu)$ crystal.

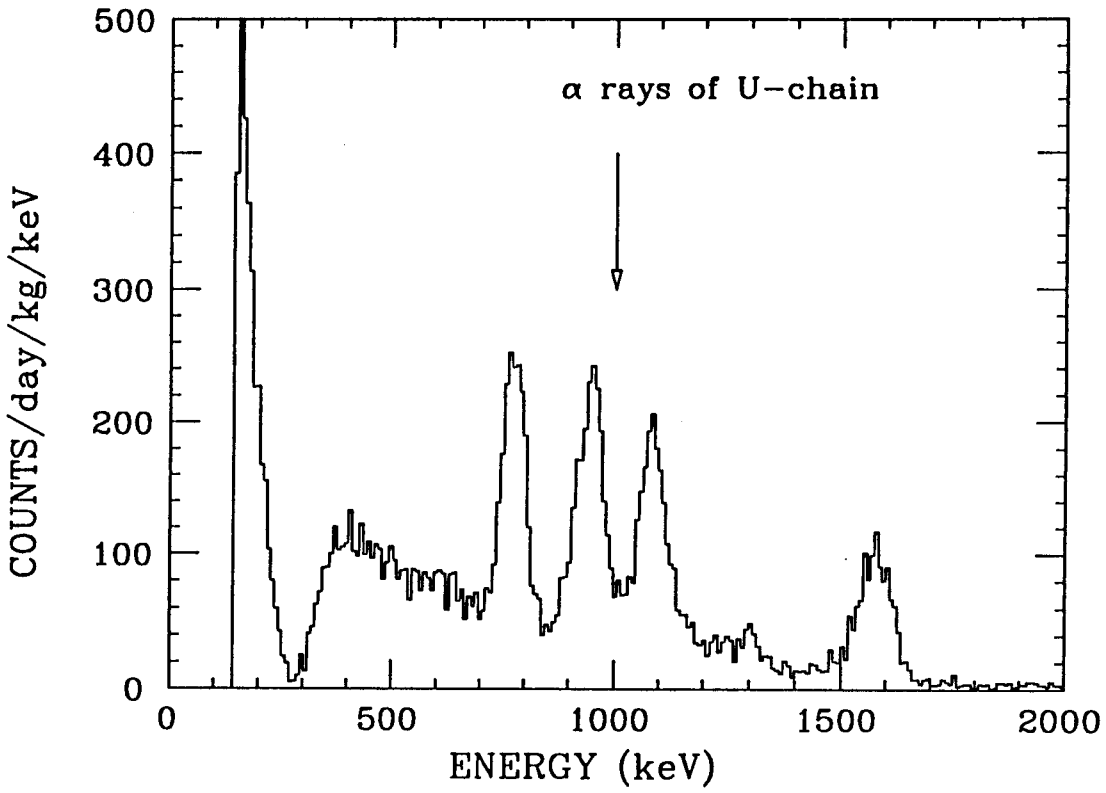

Figure 4.3: Low background energy spectrum in the high energy region for the live time of 0.7kg ·day. There are prominent peaks from U-chain radio activities.

The low energy spectrum of $CaF_2(Eu)$ for the live time of 0.25kg·day is shown in Fig.4.4. The event rate at the threshold energy (20keV) was around 200 counts /day /keV /kg. In order to set certain limit on the density of WIMPs, the background level has to be reduced by a factor of 50 and the noise level has to be lowered below 10keV.

The most of the continuous background is due to the Compton scattering of high energy γ rays, for example, ^{40}K (1461keV) and ^{214}Bi (609keV,1120keV,1764keV). Since the $CaF_2(Eu)$ has small Z number, the ratio of Compton scattering and photo-peak is large. These events must be reduced by constructing a more effective anti-Compton counter system than the present system.

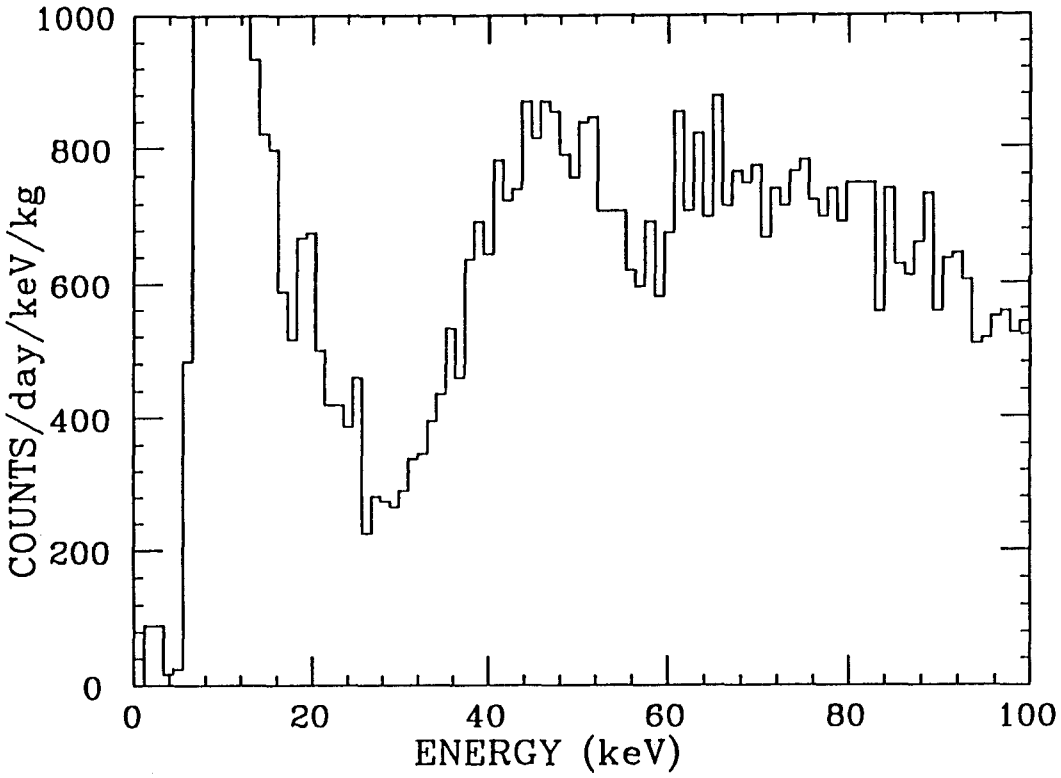

Figure 4.4: Low background energy spectrum in the region of interest for WIMPs search for the live time of 0.26kg ·day. The energy threshold was 15keV and the background rate was 300 counts/keV/day/kg. The γ ray from ^{210}Pb and the X rays from U-chain can be seen. This background level is remarkably low for the measurement in the overground laboratory, but it is not usable to set limit on the WIMPs density.

The effect of anti-Compton method is shown in Fig.4.5. The energy threshold of NaI(Tl) was 10keV and veto duration was 20μsec. It was found that the background was reduced by a factor 1/20. However this background rate is too large to search for the WIMPs candidates. The origin of these continuous background is expected as follows.

1. **Compton continuum of high energy γ rays**

   Since Z number of CaF_2 is small, the photopeak-Compton ratio of the detector is quite small. To reduce the Compton continuous background, the anti-Compton system is effective, however, all the present detectors were

covered with thick Al housing plates. In order to reduce these background component more effective, the housing of the detector must be thin and be made of low Z material.

It is more effective to construct a 4π active shield system. When an additive detector is inserted between a PMT and a detector crystal, the precise information of backgrounds from the PMTs can be obtained.

2. **Nitrogen flow**

   In the present study, an effective air tight structure could not constructed. The radioactive Rn in the air can suffer the low energy background because of the Compton continuum of the high energy γ rays (609keV etc.).

To reduce the low energy background rate the following properties are required to the new detector system.

1. Thin detector housing

2. 4π anti-counter system

The newly developed detector system consists of 25 small (4.5cm cube) detectors (CaF_2(Eu)) and the anti-Compton detectors (CaF_2(pure) and CsI(Tl)). All the detectors are covered with thin films to shade scintillation lights. CsI(Tl) detectors and CaF_2(pure) light guides act as the 4π anti-counter against the Compton scattering events. The details of this detector system are described in the next section.

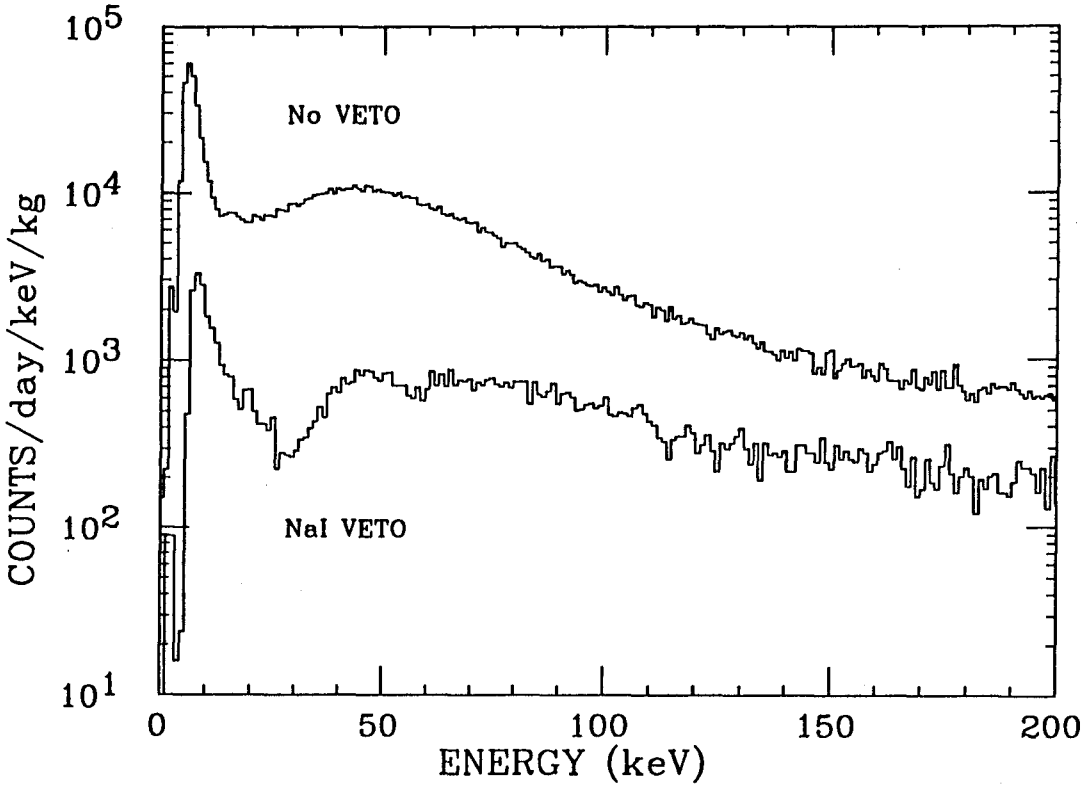

Figure 4.5: The effect of the anti-Compton counter system. The continuous background component was reduced to 1/20 by the NaI(Tl) veto. The energy threshold of the NaI(Tl) veto counter was as low as 10keV.

4.4 Future prospects of WIMPs search

4.4.1 Aims

Recently, a huge $CaF_2(Eu)$ detector system has been developed to search for WIMPs. This detector system is designed so as to have a higher sensitivity for spin-coupled WIMPs candidates than the NaI(Tl) detectors of ELEGANTS V. The aims of this study are listed as follows.

1. Search for spin-coupled WIMPs with the elastic scattering of ^{19}F. The previous excluded region of spin-coupled WIMPs by NaI(Tl) is $\Omega_\chi > 100$ at $m_{\nu_M} = 200$GeV by elastic scattering of ^{23}Na and $m_{\nu_M} = 500$GeV by inelastic scattering of ^{127}I. The first goal of this study is to set a stronger limit on Ω_χ by one order of magnitude than the previous study.

2. Search for spin-coupled WIMPs by measuring annual modulation of the recoil spectrum. The excellent statistic accuracy is needed in order to set a stringent limit on the density of WIMPs candidates. The last goal of this study is to set the limit to be $\Omega_\chi < 1$.

4.4.2 Requirements

The goal of this system is to achieve sensitivity of about $\Omega_\chi = 10$ for simple elastic scattering measurement (one order improvement) and $\Omega_\chi = 1$ for annual modulation measurement. The limits on the WIMPs candidates depend on the event rate of the unknown continuous background. An extremely low background is needed in the energy region below around 20keV. The backgrounds due to natural radioactivities and cosmic rays are more than $10^7 \sim 10^8$ events per day without any shields at the sea level laboratory. Moreover the effects of thermal and fast neutron is the most serious problem because the elastic scattering of neutron is the most probable candidate of the fake events of the DM scattering.

It is important to use odd-A nuclei with large nuclear sensitivity and to use detectors with large detector sensitivity. The former is defined as figure of merit in eq.(4.1). The CaF_2(Eu) detector has shown to be a quite suitable detector from the view points of both the nuclear sensitivity and detector sensitivity as discussed in the previous section. High sensitivity detectors require the low background rates, large acceptance and high efficiency and large amounts of target nuclei. In the present section the sensitivities of the new detector system of CaF_2(Eu) are discussed.

1. **Low background**

   Radioactive contaminants in all materials have been examined. The amount of U and Th chain contaminants in the detector crystals are found to be less than 370mBq/kg. The whole detectors are kept in an air tight box

made of acrylic plates. Pure nitrogen gas is introduced to replace the air containing natural Rn gas. It reduces the density of radioactive Rn gas less than 5Bq/m^3. The whole system is shielded by 5cm thick OFHC bricks and 5cm thick lead bricks. The neutrons which are created out of the shield are absorbed by Cd plate and borated plastic (15% of boron).

2. **High selectivity of the events from backgrounds**

   The most probable background events are due to the Compton continuous spectrum and the elastic scattering of neutrons.

   First, the contribution of the Compton scattering can be estimated by the Monte Carlo simulation based on the measured yield of the high energy γ rays. To make accurate estimation of the γ ray peaks, the CaF_2(Eu) crystals are relatively large volume. Pure CaF_2 crystals are put both sides of the CaF_2(Eu) crystal in order to estimate the effect of the backgrounds from the PMTs.

   Second, the elastic and inelastic scattering of neutrons can be removed by the coincidence measurement. Fast neutrons make subsequent scattering with the other detectors. Thus the neutrons can be reduced by eliminating the high multiplicity event. If the fast neutrons are subsequently thermalized and captured in the shielding or in the detector, they produce subsequent β ray and high energy γ rays.

3. **Large mass (Good statistic accuracy)**

   The excellent statistic accuracy is needed to set the stringent limit on the density by measuring the annual modulation. The event rate of DM-nucleus scattering varies periodically (for further discussion see the next section). The periodical modulation of the event rate gives the limit on the WIMPs scattering. The sensitivity of this experiment roughly depends on $1/\sqrt{N_i}$,

where N_i is the daily event rate of the unknown background. Thus a large detector mass is needed to obtain the stringent limits on the WIMPs candidates.

4.4.3 Detectors and shields

As shown in Fig.4.6, the new CaF_2 system consists of three types of detectors, the CaF_2(Eu) detectors, the CaF_2(pure) detectors and CsI(Tl) detectors. They

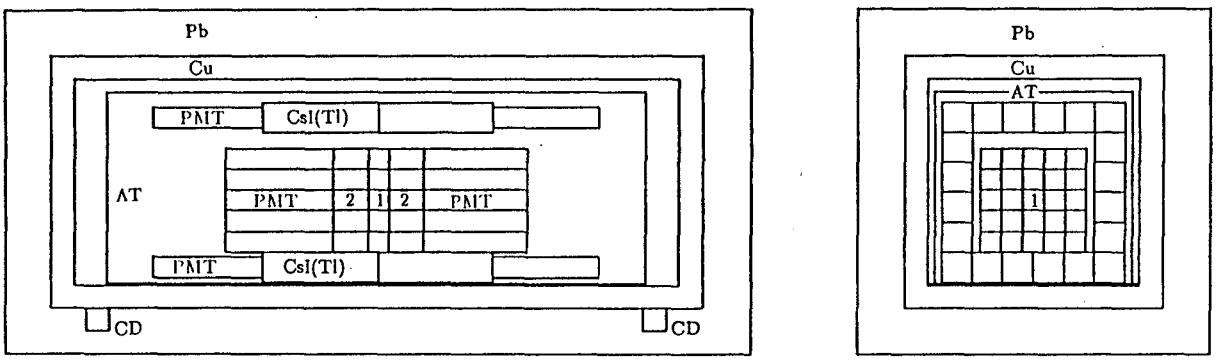

Figure 4.6: New experimental system of CaF_2(Eu) for WIMPs search.
1: CaF_2(Eu) scintillator; 2: CaF_2(pure) light guide; Pb: lead shield; Cu: OFHC shield; CsI: CsI(Tl) scintillator; AT: air tight box; CD: cable drain; PMT: photo multiplier tubes.

are placed inside the air tight box and shields. In what follows configurations and properties of the components of this system are briefly described.

1. **Detectors**

   The detector system consists of three types of scintillators, i.e. the CaF_2(Eu)

detectors, the CaF_2(pure) detectors and CsI(Tl) detectors.

The main detectors consists of 25 modules of CaF_2(Eu) crystals of the 4.5cm $\times$4.5cm $\times$4.5cm provided by BICRON Co Ltd (total mass is 7.27kg). Each CaF_2(Eu) module is viewed at both ends by low-background 4.5cmϕ PMTs H1161 provided by Hamamatsu photonics Co. Ltd. Here K-free glass is used as the window of the PMT. A light guide of 7.5cm $\times$4.5cm $\times$4.5cm pure CaF_2 is inserted between the CaF_2(Eu) and the PMT. The pure CaF_2 crystals act as a active shield against the background from the photomultipliers.

Since the optical cement does not transmit the UV light which is emitted by CaF_2(pure), the CaF_2 crystals and PMTs are connected with optical grease. The PMTs are supported by acrylic pillows and tied up with thin wire.

The central CaF_2 array is surrounded by CsI(Tl) scintillators of the 6.5cm $\times$6.5cm $\times$25cm. Each CsI(Tl) is viewed at one end by a 5.1cmϕ PMT H1161. The PMT is connected with the CsI(Tl) crystal by optical cement. These scintillators act as the active shield against high energy γ rays. To guarantee the high efficiency of Compton γ rays, all the crystals are not covered with aluminum case but with thin film for a shield against light.

2. **Air tight box**

Whole the detector array is kept in the air tight box to keep away the radioactive Rn gas in the air. The air tight box is made of 5mm thick acrylic plates whose dimension is 1160mm(L)$\times$420mm(H)$\times$420mm(W). A 5mm thick SUS plate is used for the bottom of the air tight box to keep the strength. Two connector panels for high voltage and signal cables are attached on the both sides of the box.

3. **Shields (γ rays)**

Whole the system is shielded by 5cm thick OFHC bricks and 10cm thick

lead bricks. External γ rays due to ^{40}K, U, Th chains are reduced by the factor of 10^{-3}. The amounts of U and Th chain activities are examined by ELEGANTS IIIs [49] resulting that these contaminants are less than a few ppb.

4. **Shields (neutrons and cosmic rays)**

   The fast neutrons are created by interactions of cosmic ray muons in the surrounding materials. Two ways for eliminating the neutron background are considered according to where the neutrons are created, that is, out of the shield and in the shield.

   If a neutron is created in the shield (OFHC or lead) by the interaction of the cosmic muons, the cosmic rays which cause the neutron creation can be detected by plastic scintillator. The cosmic muon decays after being captured or stopped, thus the delayed neutron events is eliminated by a muon veto for relatively long time duration $\simeq 10 \sim 20\mu$sec.

   The fast and thermal neutrons created out of the shield can be absorbed by borated polyethylene placed out of the lead shield.

   The high energy γ rays which are caused by thermal neutron capture can be reduced by the anti-coincidence with the detector array because the high energy γ rays make high multiplicity events.

4.4.4 Data taking and analyzing system

The data taking system consists of two parts. One is the electronics and CAMAC system, and the other is the software system. There are 50 energy and 50 gate signals from the 50 PMTs of the 25 CaF_2(Eu) modules, and 40 energy signals from 40 PMTs of the 40 CsI(Tl) modules. All the pulse height informations are acquired by the UNIX mini-computer through the CAMAC controller, and are

recorded into the 400MB hard disk in event-by-event mode. The data on the hard disk are transferred to 8mm video tape to be sorted for off-line analysis using the UNIX mini-computer system.

The continuous spectrum of β rays from the decay of ^{214}Bi suffers the event rate even in the low energy range. As for this background from the air, it can be reduced by sufficient nitrogen circulation. It is important to reduce this background which is contained in the CaF_2(Eu) crystal. This background can be removed to observe the α rays. As shown in Fig.4.7, ^{214}Bi decays to ^{214}Po. ^{214}Po emits α ray in a few hundred micro seconds. Consequently these background events can be reduced if this delayed α ray is detected. In principle, since the origin of this background is in the detector crystal, the delayed α ray can be surely detected.

To catch such a delayed events, the data taking system has three gate conditions. The first ADC gate is the one for the primaly events. The second and third ADC gates are opened in case of the delayed events take place in 2msec.

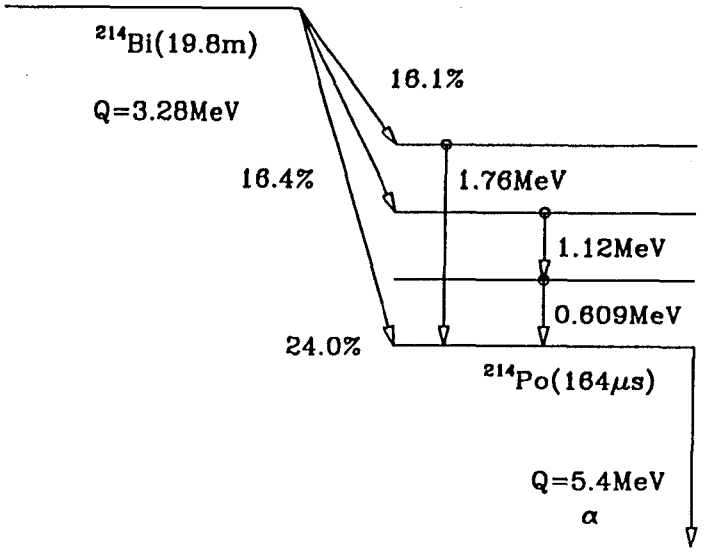

Figure 4.7: Decay scheme of ^{214}Bi $\rightarrow ^{214}$Po [41]. The β rays and the Compton scattering of γ rays may suffer the low energy background. The delayed α ray event from ^{214}Po occurs within a few hundred micro seconds.

4.5 The annual modulation of WIMPs

4.5.1 Introduction

More stringent limits on the WIMPs candidates can be derived from the small annual modulation of the event rate and the spectrum of WIMPs.

The annual modulation of the WIMPs signal results from the relative motion to the galaxy co-ordinate system. The velocity of the sun relative to the galaxy co-ordinate system is 220kms^{-1} and the velocity of the earth relative to the sun is 30kms^{-1}. Since the orbital plane of the earth is inclined at 60° to the direction

which the sun moves, the velocity of the earth relative to the galaxy co-ordinate system varies periodically with the period being one year. Consequently there is an annual modulation in both the WIMPs flux and their mean incident energy.

The velocity relative to the galaxy co-ordinate system is the highest in the beginning of June and the lowest in the beginning of the December. However, the difference is quite small, thus the difference of the WIMPs signal must be discussed with a year-long modulation.

The WIMPs signal is assumed to be composed of two parts as,

$$S(t) = S_0 + S_m \cos(\omega t). \tag{4.4}$$

Where t is the unit of day and $\omega = 2\pi/365$. t is taken to be zero when the earth's velocity is at a maximum, on June 2 ± 1.3days. The first term in eq.(4.4) is assumed to be a Poisson random variable. It implies that the variance of the event rate S_0 is equal to its mean:

$$\sigma^2(S_0) = < S_0 > . \tag{4.5}$$

The second term in eq.(4.4) is the absolute modulation rate. Strictly speaking, S_m should be treated as a random variable, but in case of interest, $S_m \ll < S_0 >$, the modulation S_m may be treated as a constant, i.e., its variable may be neglected.

The energy dependence of Jun-Dec difference is shown by K.Freese et al. [50]. It is clearly shown that the largest difference is given in the low energy range. Moreover, it shows that the modulation between June and December is too small to give a significant limit for a few years measurement. Thus the bulk of the modulation in wide energy range must be observed for all through the year.

The actual observed event rate is composed by the WIMPs signal and the background as,

$$D(t) = S_0 + B(t) + S_m(t). \tag{4.6}$$

The information about the modulation is extracted by the random variable which indicates the modulation significance as,

$$R = \frac{X}{\sigma(X)}. \tag{4.7}$$

X is the random variable which projects out the modulating portion of the data defined as,

$$X = \sum 2\cos(\omega t_i) D(t_i, \tau), \tag{4.8}$$

where $D(t_i, \tau)$ is the number of events in a time bin of width τ centered at time t_i,

$$D(t_i, \tau) = \int_{t_i - \tau/2}^{t_i + \tau/2} dt D(t_i, \tau)$$

The average of R can be easily derived when the bin width τ is much shorter than the modulation period P, e.g., τ = 1day and the modulation period is 1yr. Then

$$< R >= \frac{365 S_m N^{1/2}}{\sqrt{2 < D_{ann} >}}, \tag{4.9}$$

where N is the number of years the experiment runs, $< D_{ann} >= \sum < D(t) >$ is the sum of the daily data. For a year-long measurement, $< D_{ann} >$ is expected, so that, to an excellent approximation,

$$r \equiv \frac{x}{\sqrt{2 d_{ann}}} \tag{4.10}$$

may be regarded as a measurement of R. Here x and d_{ann} are the measurements of X and $D(t)$, respectively. The significance is related with the confidential level as, $r = 1(84\%)$, $r = 1.29(90\%)$, $r = 1.64(95\%)$, respectively.

The annual modulation of the background can be examined by the random variable, $Y \equiv \sum 2\sin(\omega t) D(t_i)$. If a measurement of X is statistically significant but a measurement of Y is not, this may be regarded as evidence that there is no annual modulation in the background [50]. If small modulation is observed, its origin must be carefully examined. One of the candidates of the origin of the

annual modulation whose peak is in the beginning of June is, of course, the WIMPs signal There are a number of sources of background which have systematic time dependences.

1. Solar neutrino

   The flux of solar neutrino can have an annual modulation because the orbit of the earth is elliptical. However, since its phase is opposite the one of WIMPs, this modulating component can be examined comparing the data between March and August with the data between September and February.

2. Cosmic rays

   The flux of cosmic rays with the energy below 10GeV has a time-dependence. But it is due to the 11-year cycle of the solar activity. Thus the solar neutrino gives little contribution to the annual modulation.

3. Seasonal variations in temperature

   The variations in temperature cause the drift of the pulse heights of the detectors. This effect can be avoided by the temperature control by air-conditioners.

In principle, it is believed that their contributions to the background are subdominant in comparison with natural radioactive contamination.

4.5.2 Estimation of the annual modulation for new CaF_2(Eu) system

For the practical measurement, the event rate in the energy region $E_{\rm th} < E_R < E_{\rm max}$ should be examined. The maximum recoil energy is given as, $E_{\rm max} = \frac{2m_\chi m_N}{(m_\chi+m_N)^2} m_\chi \beta_{575}^2$, where $\beta_{575} = 575 {\rm kms}^{-1}/c$ is the galactic escape velocity.

The energy threshold affects the amplitude of the modulation. The high energy threshold hides the WIMPs recoil spectrum and the only small fraction of the

modulation can be observed. The effect of energy threshold is given by the ratio of the threshold energy to the maximum recoil energy of WIMPs by a factor A^2, defined as

$$A^2 \equiv \frac{3E_{th}}{rm_\chi \bar{v}^2} \tag{4.11}$$

[50].

The annual modulation is the largest for $A^2 \simeq 1$ and the large value of $A(> 8)$ cannot give any effective limit on the WIMPs. The estimation of the sensitivity was given with several energy threshold and WIMPs mass (see table 4.3). (For the evaluation of modulation significance, $< R >$, see Appendix A.2.)

Table 4.3: The estimations of the significance of annual modulation, $< R >$. The detector is CaF_2(Eu) of 7.27kg. The WIMPs candidates are ν_D (a) and ν_M (b). The masses of WIMPs are 50GeV, 100GeV,500GeV. Assumed background rate is 10events/kg/day/keV, which has the constant value in the range of interest. The energy thresholds are 5keV, 7keV and 10keV in electron equivalent.

(a)	Energy threshold (keV)		
m_ν(GeV)	5keV	7keV	10keV
50	1.40	—	—
100	1.02	0.73	—
500	0.31	0.23	0.18

(b)	Energy threshold (keV)		
m_ν(GeV)	5keV	7keV	10keV
50	0.335	—	—
100	0.242	0.173	—
500	0.073	0.055	0.041

This table shows that quite low energy threshold is needed. In principle, such a low energy threshold measurement can be carried out because the light output of CaF_2(Eu) is sufficiently large. For ν_M search, the significance will be too small for 1 year's measurement. However, the significance is inversely proportional to the square root of the background rate. Thus the strong limit ($< R > \geq 1.29$ (90% CL))

on the ν_M(spin-coupled WIMPs) can be set by the estimation of the component of the continuous background and subtraction of the background components.

Chapter 5

Concluding remarks.

1. Huge NaI(Tl) scintillators in the ultra low background and high sensitivity detector system ELEGANTS V (ELEctron GAmma-ray NeuTrino Spectrometer V) have been used to search for dark matter. The advantages of the NaI(Tl) detector are listed below.

Large number of neutron ($N_n = 74$ for ^{127}I)	→	Large cross section of vector coupled WIMPs.
100% abundance of odd-A nuclei ^{23}Na($J = 3/2$),^{127}I($J = 5/2$)	→	Large cross section of axial-vector coupled WIMPs.
Low-energy ($\frac{7}{2}^+$) state with known M1 matrix element	→	Search for axial-vector coupled WIMPs by inelastic excitation.
Large volume (36.5kg/module) Total (20 modules) mass is 770kg	→	Large acceptance.

2. The light output response of nuclear recoil in the NaI(Tl) scintillator has been obtained. It is given by $f \equiv E_o/E_R$, where E_o and E_R are the electron equivalent energy and recoil energy. The response was measured by fast neutron scattering. First, inelastic excitation of ^{127}I nucleus was measured. The output response was derived by comparing the peak shape of the γ ray following the inelastic excitation and the Monte Carlo simulation as

$$f_{\rm I} = 0.05 \pm 0.02.$$

Second, the elastic scattering of ^{127}I and ^{23}Na was measured. After the apparent background peaks were removed, the experimental data were fitted by energy spectra of recoiling ^{23}Na and ^{127}I ions due to the neutron elastic scattering. The light output responses of ^{127}I and ^{23}Na recoiling were determined as

$$f_{\mathrm{I}} = 0.05 \pm 0.02$$

$$f_{\mathrm{Na}} = 0.4 \pm 0.2.$$

It should be emphasized that the same values of f_{I} were derived from independent analyses of the inelastic scattering and the elastic scattering.

3. Low background measurement of the large NaI(Tl) detector was carried out to study elastic scattering of dark matter in the Kamioka underground laboratory. The nine best modules of NaI(Tl) were used for the measurement. The central one acted as the WIMPs detector and the surrounding 8 modules acted as the active shield against the high energy γ rays and cosmic rays. Extremely low background ($\sim$ 8events/day/keV/kg) in the low energy region and low noise ($\sim$ 5keV) were achieved even with a huge (36.5kg) NaI(Tl) scintillator. The form factor of ^{127}I in the scattering reduces the scattering cross section. Consequently only ^{23}Na is useful to search for the axial vector-coupled WIMPs with the NaI(Tl) scintillator.

4. The spin-coupled WIMPs candidates were studied by the axial-vector excitation of ^{127}I nuclei. This method has a great advantage that the nuclear matrix element of the scattering is derived from the M1 γ transition rate. The first excited state of ^{127}I (57.6keV) was studied with the NaI(Tl) scintillators of ELEGANTS V. The 17 modules with the lowest background rate

were selected among the total 20 modules of ELEGANTS V. The observed energy spectrum was reproduced by fitting the energy spectrum. The analysis gave much stringent limit (one order improvement) than that was given by the study of elastic scattering.

It should be emphasized that this limit is based on the observed matrix element for the inelastic excitation while the previous one on the theoretically estimated one for the elastic process.

5. A CaF_2(Eu) was shown to be a quite suitable detector to search for spin-couples WIMPs candidates, because the spin matrix element for the elastic sattering is large and can be well evaluated theoretically. The detector has a large mass fraction of ^{19}F nuclei.

   The basic properties of CaF_2(Eu) were studied as listed below,

Low background	$\rightarrow$	High purity (99.999%)
Easy to handle	$\rightarrow$	Non-hygroscopic
Large light output (50% of NaI(Tl))	$\rightarrow$	Low energy threshold $E_{\rm th} \simeq$4keV
Light output response of α ray	$\rightarrow$	$f_\alpha = E_\alpha / E_o = 0.17$

   A CaF_2(pure) is not suitable for WIMPs search because the light output is much smaller than CaF_2(Eu). It was shown that the CaF_2(Eu) detector is quite promising detector to search for spin-coupled WIMPs candidates.

6. The huge (7.27kg) CaF_2(Eu) detector system is now under construction. It consists of 25 CaF_2(Eu) crystals and 50 CaF_2(pure) light guides. They are viewed by PMTs from both sides of the detector. Each size of the CaF_2(Eu) is 45mm $\times$45mm $\times$45mm (total mass=7.27kg). 16 modules of CsI(Tl) are used for active shield. All the detectors are contained in the air tight box.

Pure nitrogen gas is introduced into it to purge out the radioactive Rn gas. The passive shields are 5cm thick OFHC bricks and 10cm thick lead bricks.

The main property of this system is that the main CaF_2(Eu) scintillator is surrounded by 4π active shield. Thus the high selectivity of the events is expected. All the materials of the detector have been examined to check contamination of natural radioactivities. The amounts of U and Th chain isotopes are found to be less than 370mBq/kg.

7. The annual modulation of the recoil energy spectrum of WIMPs has been estimated for the new CaF_2(Eu) system. The motion of the earth relative to the galaxy makes the annual modulation of the event rate of the WIMPs-nucleus interaction. The feasibility of the search for spin-coupled WIMPs by annual modulation has estimated. The vector-coupled WIMPs (ν_D) can be excluded from the candidate of dark matter by a year long measurement. The strong limit on the density of the axial vector-coupled WIMPs (ν_M) can be derived by long term measurement for a few years.

Appendix A

Evaluation of a limit on the density of WIMPs

A.1 Limit by simple elastic scattering

The limits on the WIMPs density is derived by comparing between the measured event rate and the predicted event rate of WIMPs at the measured energy region. The predicted recoil energy spectrum is derived assuming that the low energy scattering in general is isotropic in the center of mass, so that differential event rate $dR/d\Omega = 4\pi$. The predicted nuclear recoil spectrum is [1]

$$\frac{dR}{dE_R} = c_1 \frac{R_0}{rE_0} \exp\left(\frac{-c_2 E_R}{rE_0}\right) |F(q)|^2, \tag{A.1}$$

where $E_0 = m_\chi \beta_0^2/2$ is the average kinetic energy of WIMPs, $\beta_0 = v_0/c$ is the average velocity of WIMPs, m_χ and m_N is the masses of WIMPs and detector nucleus, and $r = 4m_\chi m_N/(m_\chi + m_N)^2$. The case $c_1 = c_2 = 1$ gives the stationary-earth spectrum, while values $c_1 = 0.8$ and $c_2 = 0.64$ give a good approximation of the WIMPs recoil spectrum, which includes the earth's galactic motion. This recoil spectrum is interpreted to the observed spectrum in a scintillation detector as,

$$\frac{dR}{dE_{ob}} = \frac{1}{f}\frac{dR}{dE_R}, \tag{A.2}$$

provided that the light output does not differ in the observed energy region.

The limit on the event rate dR/dE_{ob} is evaluated by comparing a given background spectrum. For the simple case that the background falls less steeply than the recoil spectrum, an approximate limit of observability can be defined when the recoil spectrum passes through the intersection of the background spectrum with the measurement threshold, $E_{\rm th}$. Thus eq.(A.1) can be rewritten as

$$\frac{R_0}{r} = \left(\frac{dR}{dE_{ob}}\right)_{\rm th} \frac{f}{c_1} \exp\left(\frac{c_2 E_{R\rm th}}{E_0 r}\right) \frac{1}{|F(q_{\rm th})|}. \tag{A.3}$$

The total event rate R_0 in the detector is given as,

$$R_0 = n_0 \frac{2}{\sqrt{\pi}} \beta_0 c \sigma_\chi \frac{6 \times 10^{26}}{A} \ \sec^{-1}\mathrm{kg}^{-1}. \tag{A.4}$$

Where $\beta_0 \equiv v0/c$ stands for the mean velocity of WIMPs, σ_χ is the elastic cross section of WIMPs and n_0 is the number density of WIMPs related to the mass of WIMPs particle as,

$$n_0 = \frac{\rho_\chi}{m_\chi}. \tag{A.5}$$

From the eqs.(A.1),(A.4) and (A.5), the limit on the density of a WIMPs candidate is derived as,

$$\rho_D = \left(\frac{dR}{dE_{ob}}\right)_{\rm th} \frac{f}{c_1} \frac{4.92 \times 10^6}{\beta_0} \frac{E_0 r m_\chi A}{a \sigma_{38}} \exp\left(\frac{c_2 E_R}{E_0 r}\right). \tag{A.6}$$

Where $\sigma_{38} = \sigma_\chi \times 10^{38}\mathrm{cm}^2$ and a is the mass fraction of the isotope A in the detector.

A.2 Estimation of the annual modulation

When one estimates the feasibility of the WIMPs search with the CaF_2(Eu) detector system, to derive the expected modulation significance R gives a good information. The WIMPs will be assumed to have an isotropic velocity-independent cross section, which can be parametrized as [50],

$$\sigma = 5.2 \times 10^{-40}\mathrm{cm}^2 \cdot \frac{m_\chi m_N r}{\mathrm{GeV}^2} Q^2, \tag{A.7}$$

where Q is a parameter which depends on the detector nucleus and the WIMPs identity. The scattering parameter Q for ν_D and ν_M, for example, are

$$Q^2_{\nu_D} = \left\{N_n - (1 - 4\sin^2\theta_W)N_p\right\}^2, \tag{A.8}$$

$$Q^2_{\nu_M} = 20.5\lambda^2 J(J+1). \tag{A.9}$$

Where these equations are normalized so that the values of $\lambda^2 J(J+1)$ given by Goodman and Witten [44] and Drukier, Freese and Spergel [52] should be used [50]. For example, $\lambda^2 J(J+1) = 0.91$ for ^{19}F.

To evaluate the modulation significance R, the mean of R can be given by the following three assumption; i) the expected background is much greater than the time-averaged WIMPs signal, ii) the background is much smaller than the time-averaged WIMPs signal, iii) the background and the time-averaged WIMPs signal are comparable ($0.1 \leq S_0/B \leq 10$).

In the first case, the modulation significance is given as [50],

$$< R >_B = 0.041 r Q^2 \beta(A^2)\sqrt{B_{10} m_{det} t}\,\rho_{0.4}\bar{v_{270}}, \tag{A.10}$$

where the halo velocity dispersion $\bar{v} = 270\bar{v_{270}}\mathrm{kmsec}^{-1}$, the local halo density $\rho_\chi = 0.4\rho_{0.4}\mathrm{GeV/cm}^3$, the detector mass m_{det} and $< B >= 10B_{10}$ is the total background rate in the region $E_{\mathrm{th}} \geq E \geq E_{\mathrm{max}}$. The function β gives the absolute modulation of the signal at energy threshold A^2 as a fraction of its value at zero threshold.

In the second case, the modulation significance is given as,

$$< R >_S = 0.23 r^{1/2} Q \alpha(A^2)\sqrt{m_{det} t \rho_{0.4}\bar{v_{270}}}, \tag{A.11}$$

where α gives the modulation significance when the background is smaller than the WIMPs signal defined as,

$$\alpha \equiv \frac{\beta(A^2)}{\gamma(A^2)^{1/2}}. \tag{A.12}$$

Where $\gamma(A^2)$ gives the signal at energy threshold A^2 as a function of its value at zero threshold.

The functions, α, β and γ are shown in Fig.A.1 for reader's guide.

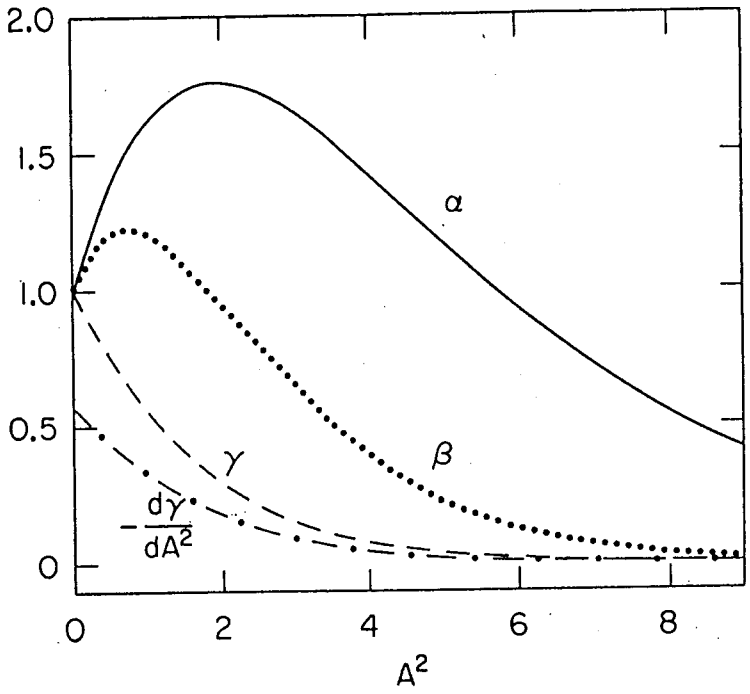

Figure A.1: Dimensionless measures of the WIMPs signal (γ), the signal per unit energy ($-d\gamma/dA^2$), and the modulation significance when the signal is much greater than (α), or much less than (β) the background. (A quotation from Phys. Rev. **D37** (1988) 3388) [50].

In the second case, it may be the most probable case, one should use the exact expression for the modulation significance as,

$$< R >= \frac{< R >_S < R >_B}{\sqrt{< R >_S^2 + < R >_B^2}}. \qquad \text{(A.13)}$$

The significance is related to the confidence level: $< R >$=1(84%), 1.29(90%), 1.64(95%), 2.00(97.7%) and 3.00(99.9%). A measurement of $< R >$, ie $r = 1.3$, would be a fairly reliable indicator of modulation.

Bibliography

[1] J.R.Primack D.Seckel and B.Sadoulet, Ann. Rev. Nucl. Part. Sci. **38** (1988) 751;
P.F.Smith and J.D.Lewin, Phys. Rep. **187**No.5 (1988) 203.

[2] G.Steigman, Nucl. Phys. **B31**(Proc. Suppl.) (1993) 343.

[3] J.P.Ostriker et al., Astophys. J. **193** (1974) L1.

[4] J.Einasto et al., Nature **250** (1974) 309.

[5] A.Gould, Astrophys. J. **403** (1993) 37.

[6] J.Yang et al., Astrophys. J. **251** (1984) 493.

[7] H.Y.Cheng, Phys. Rev. **D36** (1987) 1649.

[8] R.Mayle et al., Phys. Lett. **B203** (1988) 188.

[9] F.T.Avignon III et al., Phys. Rev. **D35** (1987) 2752;
K.van Bibber et al., Phys. Rev. **D39** (1989) 2089.

[10] M.Beck et al., Talk given in TAUP'93 Phys.Lett **B**(Proc. Suppl.) to be published.

[11] F.A.Danevich et al., Talk given in TAUP'93 Phys.Lett **B**(Proc. Suppl.) to be published.

[12] G.F.Smoot et al., Astrophys. J. **396** (1992) L1.

[13] E.L.Wright et al., Astrophys. J. **396** (1992) L13.

[14] J.G.Bartlett and J.Silk, Astrophys. J. **407** (1993) L45.

[15] Y.Suzuki, 'Frontiers of Neutrino Astrophysics', Ed. Y.Suzuki and K.Nakamura, Universal Academy Press Inc. (1993) 61, and the references therein.

[16] R.Davis, 'Frontiers of Neutrino Astrophysics', Ed. Y.Suzuki and K.Nakamura, Universal Academy Press Inc. (1993) 47.

[17] P.anselmann et al., GALLEX Collaboration, Phys. Lett. **B285** (1992) 376.

[18] R.L.Gilliland et al., Astrophys. J. **306** (1986) 703.

[19] M.Mori et al., Phys. Lett. **B270** (1991) 89.

[20] M.Mori et al., Phys. Lett. **B289** (1992) 463.

[21] L.Krauss, Phys. Rev. Lett. **64** (1990) 999.

[22] J.Ellis et al., Phys. Lett. **B245** (1990) 251.

[23] D. O. Caldwell et al., Phys. Rev. Lett. **61** (1988) 510;
D. Reusser et al., Phys. Lett.**B255** (1991) 143.

[24] M.Beck et al., Phys. Lett. in print.

[25] D.O.Caldwell et al., Phys. Rev. Lett.**65** (1990) 1305.

[26] D. O. Caldwell, Nucl. Phys. **B**(Proc. Suppl.)**31** (1993) 371.

[27] M.Minowa et al., 'Frontiers of Neutrino Astrophysics', Ed. Y.Suzuki and K.Nakamura, Universal Academy Press Inc. (1993) 593.

[28] BRS Collaboration, Phys. Lett. **B293** (1992) 460;
A.Bottino et al.BRS Collaboration, Phys. Lett. **B295** (1992) 330.

[29] K. Fushimi, H. Ejiri, H. Kinoshita, N. Kudomi, K. Kume, K. Nagata, H. Ohsumi, K. Okada, H. Sano and J.Tanaka, Phys. Rev. **C47** (1993) 425.

[30] Lindhard et al., Mat. Fys. Med. Vid. Selsk. **33** (1963) 10.

[31] B.Sadoulet et al., Astrophys. J. Lett. **324** (1988) L75.

[32] B.Sadoulet, 'Frontiers of Neutrino Astrophysics', Ed. Y.Suzuki and K.Nakamura, Universal Academy Press Inc. (1993) 371.

[33] M. N. Erduran and R. B. Galloway, J. Phys. G: Nucl. Phys. **12** (1986) 965.

[34] J. H. Towle and W. B. Gilboy, Nucl. Phys. **32** (1962) 610.

[35] U.S.Atomic Energy Commission, "Neutron Cross Sections".

[36] G.Gerbier, Private communication (1993).

[37] Beijing, Paris, Roma, Saclay collab., talk given in TAUP93, Phys.Lett **B**(Proc. Suppl.) to be published.

[38] H. Ejiri, K. Higa, T. Kamada, H. Kobiki, K. Matsuoka, K. Okada, H. Sano, T. Shibata, T. Shima, N. Tanabe, J. Tanaka, T. Taniguchi, T. Watanabe and N. Yamamoto, Nucl. Instr. Meth. **A302** (1991) 304.

[39] H. Ejiri, K. Fushimi, T. Kamada, H. Kinoshita, H. Kobiki, H. Ohsumi, K. Okada, H. Sano, T. Shibata, T. Shima, N. Tanabe, J. Tanaka, T. Taniguchi, T. Watanabe and N. Yamamoto, Phys. Lett. **B258** (1991) 17;
Phys. Rev. **C44** (1991) 502.

[40] K.Matsuoka, N.Tanabe, T.Watanabe and H.Ejiri, OULNS Annual Report, Osaka Univ. (1988) 25.

[41] Table of Isotopes, 7th Edition 1978, edited by C. M. Lederer and V. S. Shirley, John Wiley & Sons, INC, New York.

[42] J.Engel, Phys.Lett.**B264** (1991) 114.

[43] H.Ejiri, K.Fushimi and H.Ohsumi, Phys. Lett. **B317** (1993) 14.

[44] M.Goodman and E.Witten, Phys. Rev. **D31** (1985) 3059.

[45] E.W.Kolb and K.A.Olive, Phys. Rev. **D33** (1986) 1201; **D34** (1986) 2531.

[46] H.Ejiri ,H.Kinoshita, H.Sano and H.Ohsumi, Phys. Lett. **B282** (1992) 281

[47] J. Ellis and R. Flores, Nucl. Phys. **B307** (1988) 883;
Phys. Lett. **B263** (1991) 259.

[48] A. K. Drukier and L. Stodolsky, Phys. Rev. **D30** (1985) 2295.

[49] N.Kamikubota et al., Nucl. Instr. and Meth. **A245** (1986) 379;
H.Ejiri et al., Nucl. Phys. **A448** (1986) 271;
H.Ejiri et al., J. Phys. **G13** (1987) 839;
H.Ejiri et al., Nucl. Instr. and Meth. **A302** (1991) 482.

[50] K.Freese et al., Phys. Rev. **D37** (1988) 3388.

[51] J.I.Collar et al., Nucl. Phys. **B**(Proc. Suppl.)**31** (1993) 377.

[52] A.K.Drukier et al., Phys. Rev. **D33** (1986) 3495.

Acknowledgement

The author is especially grateful to Professor H.Ejiri for valuable discussions, suggestions and his very kind encouragement during whole course of this experiment. He thanks Professor K.Okada for valuable discussions and suggestions, and his very kind encouragement, especially, in the beginning of the course of this experiment.

He also thanks Professor T.Kishimoto, Dr.'s H.Ohsumi, J.Tanaka and H.Sano for their kind collaborations and discussions. The author is deeply indebted to all other members of the Ejiri's group at Dept. Phys. and OULNS, Osaka Univ., K.Nagata, K.Kudomi, K.Kume, H.Hazama, K.Shinmyo, and T.Senoo, K.Matsuoka, K.Higa, H.Iwata, T.Mizuta and K.Onishi and M.Nagata.

The author and collaborators wish to thank Professors Y.Totsuka, K.Nakamura and Y.Suzuki, Inst. for Cosmic Ray Research for their kind arrangements and encouragements at the Kamioka underground laboratory. Thanks are due to Kamioka Mining & Smelting Co. Ltd. for the help at the Kamioka mine.

The author wishes to thank Professors T.Shibata, Y.Nagai and M.Minowa for valuable discussions and suggestions. He is especially grateful to Professors Fukushima, A.Mito and N.Saito, Dr. Shimizu and M.Shibata in Radio Isotope Center (RI center) of Osaka University for their kind arrangements for experiment and encouragements at the RI center.

The author wishes to thank his families, Minoru, Noriko, Yuji and Tane for their continuous helps and encouragements.